

PAIR CREATION BY DYNAMIC FIELD CONFIGURATIONS

**Thesis by
Hideaki Aoyama**

**In Partial Fulfillment of the Requirements
for the Degree of
Doctor of Philosophy**

**California Institute of Technology
Pasadena, California.**

**1982
(Submitted May 18, 1982)**

Acknowledgements

I would like to express my appreciation to my advisor, Dr. H. David Politzer , for his valuable advice, encouragement and support throughout the three years of my research at Caltech.

I am indebted to Dr R. P. Feynman for enlightening discussions and comments on this thesis. I acknowledge useful Tuesday lectures given by Dr. M. Gell-Mann. I also acknowledge discussions with Dr. Jan Ambjørn, Dr. Larry Yaffe, and Dr. Stephan Wolfram.

I thank Dr. Makoto Kobayashi, Dr. Taichiro Kugo and the members of the theoretical high-energy physics group of Kyoto University for discussions during my earlier years of graduate study.

I also thank the following people for making my life at Caltech pleasant and for assisting me during the final weeks of the preparation of this thesis; Roma Gaines, Rajan Gupta, Jaisam Kim, Louise Sartain, Helen Tuck , and especially, Barton Zwiebach, who took the pains of reading my manuscript. Norman Wilson and Dave Iskandar helped me start using HEP VAX and 11/45 system.

I dedicate this thesis to my parents, for their understanding and support without which I could not have pursued my Ph.D. here in U.S.A., and to my wife Michiko, for her constant love and support.

Abstract

This thesis deals with the dynamics of the classical configuration of a quantum field unstable due to pair creation. The effective action method is developed first to treat such problems for a simple two-field model. Physical quantities such as pair creation probabilities are related to a complex function called the "effective configuration," which is defined to minimize the effective action. Unitarity of the S-matrix is verified at the lowest order of the weak-field approximation. At the same order, the real valued vacuum expectation value of the quantum field, named the "real configuration," is constructed in terms of the effective configuration. An integro-differential equation for the real configuration is given and is used to show that the real configuration is causal, while the effective configuration is not. Two practical applications of the effective action method are discussed. The first deals with pair creation in an anisotropic universe, and the "real geometry" is given in terms of the "effective geometry" in the small anisotropy limit. The second deals with expanding vacuum bubbles. Corresponding to three possible situations, three kinds of field equations for each of the effective configuration and the real configuration are obtained. The behavior of the bubble is also studied by a semi-classical method, and one of the three situations is suggested to be plausible.

Table of Contents

I. Introduction

References for Chapter I

II. The Effective Action Method

1. Introduction

2. The Effective Action

3. The Transition Amplitudes and Their Unitarity

4. The Real Configuration

5. Conclusion and Discussion

Appendix. The Operator Field Equations and the Real Configuration

References for Chapter II

III. An Anisotropy Dissipation Model of the Early Universe

1. Hartle and Hu's model

2. Effective Geometry vs. Real Geometry

References for Chapter III

IV. Vacuum Bubble Expansion

1. Introduction

2. Quantum Creation and Classical Expansion of a vacuum bubble

3. Quantum Correction to the Bubble Equation of Motion
4. A Semi-Classical Analysis
5. Discussions

References for Chapter IV

I. Introduction

Quantum field theories deal with two kinds of objects: a set of particles and anti-particles, and field configurations. "Elementary particles" belong to the former kind. Most of the high energy collision experiments are aimed at examining their properties, and we have been successful, to some extent, in constructing models appropriate up to energies of ~ 100 Gev. The simplest example of a field configuration is the electro-magnetic field radiated by a classical charged source. Within the framework of quantum electro-dynamics (QED), that radiation field is described as a coherent state, that is, an eigenstate of photon annihilation operators [1]. In general, the classical electromagnetic field $F^{\mu\nu}(x)$ we observe is understood as the expectation value of the quantum field operator $\hat{F}^{\mu\nu}(x)$:

$$F^{\mu\nu}(x) = \langle \hat{F}^{\mu\nu}(x) \rangle.$$

In this sense, classical field theories are reproduced by quantum field theories in the limit of $\hbar \rightarrow 0$.

As the result of recent development of models of fundamental interactions, expectation values of quantum field operators, or field configurations, have acquired more popularity. Gravity is one of them: The quantized versions of Einstein's theory of gravity coupled with matter have been suffering from non-renormalizability. However, development in supergravity theories [2] and string theories [3] have given us a hope that someday we might have a renormalizable

quantum field theory of gravity with matter. In such a theory, the classical observable metric would be the expectation value of the metric operator.

Field configurations play important roles in unified models of elementary particles: In 1960, Nambu [4], stimulated by the Bardeen-Cooper-Schrieffer theory of superconductivity, introduced the idea of spontaneous symmetry breaking into the dynamics of elementary particles. The idea was to let the ground state be less symmetric than the Lagrangian is, by having nonzero expectation value of certain field operators. For example, the strong interaction among N -quarks has chiral $SU(N)_L \times SU(N)_R$ symmetry at the Lagrangian level, which is violated by having nonzero vacuum expectation value (VEV) of $\sum_{i=1}^N \bar{q}_i q_i$, where q_i (\bar{q}_i) is the i -th (anti-)quark field operator [5]. In the Glashow-Weinberg-Salam model [6] of weak and electromagnetic interactions, the $SU(2) \times U(1)$ symmetry is broken down to $U(1)_{e.m.}$ by a nonzero VEV of a neutral scalar field called the Higgs field [7]. In attempts to construct grand unified theories (GUTS) to describe strong, electromagnetic, and weak interactions, we are forced to introduce more VEVs of Higgs fields or bi-linear scalar products of fermionic fields to obtain non-symmetric low-energy states. Investigation of the dynamics of these VEVs, or field configurations has become necessary for understanding the phase transitions [8~10] in the early universe.

In many of the models where field configurations play an important role, quantum effects are not negligible, in some cases, even essential: In the limit $\hbar \rightarrow 0$, quantum field theories give classical field equations for VEVs of quantum field operators. When $\hbar \neq 0$, the classical field equations are modified by quantum effects, so that the behavior of VEVs, or field configurations, differ from that of classical solutions. In particular, when particle creation is possible, the classical solutions can be unstable and decay as time passes. These created particles usually occur in pairs of particle and anti-particle in order to conserve total

quantum numbers. For example, in gravity theories quantum effects are essential in blackhole evaporation by particle creation (Hawking effect [11]), and in dynamics of early universe [12] including anisotropy damping by pair creation [13]. In theories with spontaneous symmetry breaking, in some cases, the choice of the ground state can be totally governed by quantum effects [14], and pair creation during phase transitions may also be essential in understanding the dynamics.

In this thesis, we will develop the effective action method in order to study quantum effects (especially pair creation) on field configurations, and discuss two possible applications of the formalism. The effective action method is useful in the sense that it deals directly with matrix elements of quantum field operators; in the limit $\hbar \rightarrow 0$, the effective action is equal to the classical action and therefore equations for field configurations are automatically equal to classical field equations. One of the other advantages is that it provides a consistent quantum-mechanical description of the process. In particular, when the classical configuration is unstable against pair creation, it allows us to take into account the back reaction from produced pairs in a systematic way, in contrast to semi-classical methods.

In Chapter II, we investigate the effective action method in a simple two-field model that has the essential features necessary for practical applications [16]. Namely, the fields whose configurations we are interested in are bosonic and real, as the gravitational field and the real Higgs scalar fields are. When pair creation is possible, the effective action S_{eff} has an imaginary part. Thus, the matrix elements, or more precisely, Schwinger averages [15], of the real fields obtained by minimizing S_{eff} are complex. These Schwinger averages are called the effective configuration. The observable field configurations are the diagonal matrix elements, or the "expectation values" of real fields, which we name real

configurations. We derive the relation between these real configurations and the effective configurations.

Chapter III discusses an anisotropy dissipation model of the early universe [18]. In such a model, matter fields are coupled to the gravity in the conformally invariant manner. Because of this coupling, an anisotropy of the early universe is expected to decay by creation of pairs of matter fields. Hartle and Hu [13] applied the effective action method to a model with a conformal scalar field in the small anisotropy limit and obtained numerical solutions of effective configurations of the metric, which they called the effective geometry. We discuss the real configurations of the metric, which we called the real geometry.

In Chapter IV, we discuss pair creation during phase transitions between states with different VEVs of Higgs fields. The process of phase transition from a higher energy state to a lower energy state is thought to be initiated by nucleation of "bubbles" of region where the field configuration has the value of the lower energy state. At the classical level, these bubbles are thought to expand quite rapidly and leave a clean vacuum state. However, it is not necessarily so when quantum corrections are taken into account. Expanding bubbles can create pairs, quantum-mechanically. Thus, the expansion rate is expected to be slower than the classical expansion rate, and the resulting state may not be so clean. We give field equations for the field configuration by applying the effective action method developed in chapter II. A semi-classical analysis is also presented.

References for Chapter I

- [1] Glauber, Phys. Rev. 130 (1963) 2529.
- [2] P. van Nieuvenhuizen, Phys. Rep. 68 (1981) 189
- [3] J. H. Schwartz, Caltech preprint, CALT-68-905.
- [4] Y. Nambu, Phys. Rev. Lett. 4 (196) 380; Y. Nambu and G. Yona-Lasinio, Phys. Rev. 122 (1961) 345.
- [5] For example, see; S. Weinberg, "The Problem of Mass", Transactions New York Academy of Sciences.
- [6] S. L. Glashow, Nucl. Phys. 22 (1961) 579; S. Weinberg, Phys. Rev. Lett. 19 (1967) 1264; A. Salam, in "The Elementary Particle Theory" ed. by N. Svarthom (Almqvist and Wiksell, Stockholm, 1968) 367.
- [7] P. W. Higgs, Phys. Rev. 145 (1966) 1156.
- [8] M. B. Volosin, I. Yu. Kobzarev, and L. B. Okun', Yad. Fiz. 20 (1974) 1229 [Sov. J. Nucl. Phys. 20 (1975) 644].
- [9] S. Coleman, Phys. Rev. D15 (1977) 2929.
- [10] C. G. Callan and S. Coleman, Phys. Rev. D16 (1977) 1762; S. Coleman, V. Glaser, and A. Martin, Commun. Math. Phys. 58 (1978) 211; S. Coleman and F. De Luccia, Phys. Rev. D21 (1980) 3305.
- [11] S. Hawking, Nature 248 (1974) 30; Commun. Math. Phys. 43 (1975) 199.
- [12] M. V. Fischetti, J. B. Hartle, and B. L. Hu, Phys. Rev. D20 (1979) 1757; B.L. Hu, Phys. Lett. 103B (1981) 331.
- [13] J. B. Hartle and B. L. Hu, Phys. Rev. D20 (1979) 1772, and other references given in chapter III.

- [14] S. Coleman and E. Weinberg, Phys. Rev. D7 (1973) 1888.
- [15] J. Schwinger, Proc. Nat. Acad. Sci. 37 (1951) 452,455; E. S. Abers and B. W. Lee, Phys. Rep. 9C (1973) 1; B. S. Dewitt, in "General Relativity, An Einstein Centenary Survey", ed. by S. W. Hawking and W. Israel, (Cambridge University Press , London, 1979) 680.
- [16] H. Aoyama, Soryushiron Kenkyu.(Kyoto) 62 (1981) 239.
- [17] H. Aoyama, Caltech preprint, CALT-68-900 (1982).
- [18] H. Aoyama, Phys. Lett. 107B (1981) 39.

II. The Effective Action Method

1. Introduction

One of applications of the effective action method was given by Hartle and others [2~4] in their studies of the dynamics of the early universe. They calculated the one-loop contribution of the conformally invariant scalar field to the gravitational effective action S_{eff} . The production probabilities of scalar pairs are given in terms of metrics obtained by minimizing S_{eff} . Since S_{eff} had an imaginary part corresponding to the possibility of pair creation, the resulting metrics were complex, and were called the effective geometry.

Recently, we gave the real observable metric, which we called the real geometry, in terms of the effective geometry [5]. The real geometry is defined as the expectation value of the metric operator in the initial vacuum state, while the effective geometry is the Schwinger average of the metric operator between the initial and final vacuum states. Furthermore, we verified that the real geometry had no imaginary part. However, we found that the unitarity of the S-matrix is not trivial as a consequence of the complex metric. This unitarity problem was solved in reference[6], where the causal properties of the real configuration were also clarified. This chapter covers the content of the reference [6].

A typical model we consider has two fields, one of them, the β -field, whose configuration we observe, real, and the other, the φ -field, of which pairs are

created that need not be real. Further Lorentz-properties of the β - and φ -fields are left unspecified. These fields interact via a $\beta\varphi^\dagger\varphi$ coupling so that some configuration of the β -field creates pairs of φ -particle and anti-particle. As a result of the backreaction from the produced φ -pairs, the configuration of the β -field decays with time. The problem is to give a description of this decay process and also to give prescriptions to obtain various physical quantities, including pair creation probabilities. Although we confine ourselves to the case where the φ -field is bosonic, we see no difficulty in extending the results to include fermions. The renormalizability of the model is assumed for the unitarity discussion. In this two-field model, we shall call the complex function $\tilde{\beta}$ that corresponds to the effective geometry in Hartle and Hu's model the effective configuration. Similarly, we shall call the real function β^r corresponding to the real geometry the real configuration.

In Section 2, we construct S_{eff} from the generating functional of the connected Green's functions by using a Legendre transformation on the β -field. This construction gives $\tilde{\beta}$ in terms of the real external source of the β -field, B , which enforces the boundary condition on the configuration, if necessary.

In Section 3, transition amplitudes are given in terms of $\tilde{\beta}$ at the $O(\tilde{\beta}^2)$ of S_{eff} . We prove that they satisfy unitarity conditions by using the relation between $\tilde{\beta}$ and B given in the previous section. It is clarified which physical processes are taken into account at each order of the perturbative calculation of $\tilde{\beta}$.

The real configuration is discussed in Section 4. The proof of the relation between $\tilde{\beta}$ and β^r given in Ref. [5] is improved to include the contribution of multipair intermediate states. Its consequences are discussed in relation with causality, the real configuration β^r is shown to be causal, while $\tilde{\beta}$ is not.

The appendix gives discussions based on the operator field equations. The relation between β^r and $\tilde{\beta}$ given in Section 4 is reproduced by taking the initial-vacuum expectation value of the operator field equation for the β -field. Finally a word on notation: we use subscripts i, j for any labels the field operators and their matrix elements may carry, including the space-time variables. Also implicit is integration and summation over repeated indices.

2. The Effective Action

Transition amplitudes in a quantum field theory are calculated from the Green's functions with the help of reduction formulas. The Green's functions are the matrix elements of the time-ordered products of field operators between the initial vacuum $|0-\rangle$ and the final vacuum $|0+\rangle$. In the Heisenberg representation, $|0-\rangle$ is defined to be the perturbative vacuum state for $t \rightarrow -\infty$; for example,

$$N_\varphi(t=-\infty)|0-\rangle = 0, \quad (2.1)$$

where $N_\varphi(t)$ is the operator which gives the number of φ -pairs at time t . Similarly, $|0+\rangle$ satisfies

$$N_\varphi(t=+\infty)|0+\rangle = 0. \quad (2.2)$$

The Green's functions are obtained by differentiating the generating functional $Z[B, J]$ with respect to the external sources; w.r.t. B_i for the β -field and w.r.t. J_i for the φ -field. This relation between the Green's functions and Z is easily seen in the Feynman path-integral formula:

$$e^{iZ[B, J]} \equiv \langle 0+ | 0-\rangle_{B, J} = \int [d\beta][d\varphi][d\varphi^\dagger] e^{i(S[\beta, \varphi] - \beta_i B_i - J_i^\dagger \varphi_i - \varphi_i^\dagger J_i)}, \quad (2.3)$$

where $S[\beta, \varphi]$ is the bare action. We assume that the perturbation theory applies to this $S[\beta, \varphi]$. An explicit form of S is given in the appendix. Typically, the source J is zero and is therefore taken to be zero after all necessary differentiations with respect to J are performed. On the other hand, B is not set to zero since it is used to excite the β -configuration out of the initial vacuum. In cases when initial conditions on the β -configuration are desired, B enforces them.

For our purpose of dealing with the configurations of the β -field, it is most convenient to define the effective action $S_{eff}[\beta, J]$ as a Legendre transform on the B-field, but not on the φ -field:

$$S_{eff}[\tilde{\beta}, J] \equiv Z[B, J] + \tilde{\beta}_i B_i. \quad (2.4)$$

In the above, $\tilde{\beta}$ is defined by

$$\tilde{\beta}_i \equiv - \frac{\delta Z[B, J]}{\delta B_i}. \quad (2.5)$$

We shall call this $\tilde{\beta}$ the effective configuration. Using the effective action S_{eff} of (2.4), we can obtain the Green's functions by differentiating the vacuum to vacuum amplitude;

$$\langle 0+ | 0- \rangle_{B, J} = e^{i(S_{eff}[\tilde{\beta}, J] - \tilde{\beta}_i B_i)} \quad (2.6)$$

with respect to B and J , keeping in mind that $\tilde{\beta}$ is a functional of B and J according to (2.5). Because of (2.4), S_{eff} is the generating functional of connected graphs which are proper only for the β -field, i.e., do not become disjointed upon removal of a β -propagator. Some of the lower order graphs are illustrated in Fig. 1.

By using (2.3), we find that the effective configuration $\tilde{\beta}_i$ defined by (2.5) is the Schwinger average of the β -field operator $\hat{\beta}$:

$$\tilde{\beta}_i = \frac{\langle 0+ | \hat{\beta}_i | 0- \rangle_{B, J}}{\langle 0+ | 0- \rangle_{B, J}}. \quad (2.7)$$

In terms of S_{eff} , $\tilde{\beta}$ satisfies the following equation;

$$\frac{\delta S_{eff}[\tilde{\beta}, J]}{\delta \tilde{\beta}_i} = B_i. \quad (2.8)$$

The above equation follows from (2.4) and (2.5) with the help of the chain

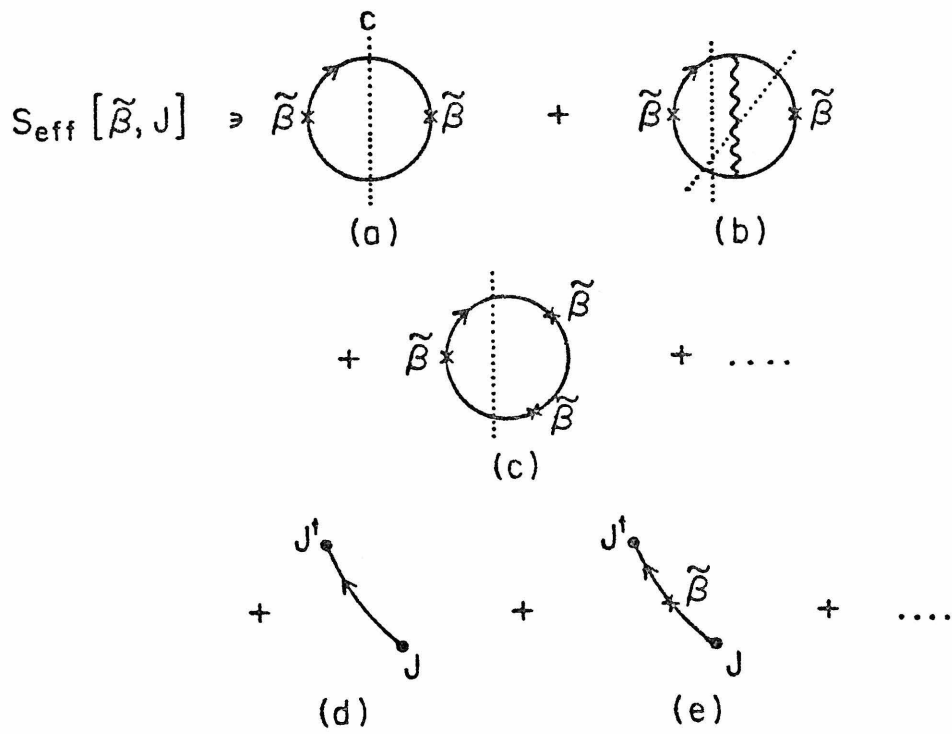


Figure 1: The lower-order Feynman graphs that represent $S_{\text{eff}}[\tilde{\beta}, J]$. The solid lines are φ -propagators and the wavy line the β -propagators. The dotted lines show possible cuts.

differentiation rule;

$$\frac{\delta S_{eff}[\tilde{\beta}, J]}{\delta \tilde{\beta}_i} = \frac{\delta B_j[\tilde{\beta}, J]}{\delta \tilde{\beta}_i} \frac{\delta Z[B, J]}{\delta B_j} + B_i + \tilde{\beta}_j \frac{\delta B_j[\tilde{\beta}, J]}{\delta \tilde{\beta}_i},$$

where the first and second terms cancel each other because of (2.5). It should be noted, however, that (2.8) is an integro-differential equation for $\tilde{\beta}$ and does not uniquely determine $\tilde{\beta}$. It seems rather difficult to find the boundary condition on $\tilde{\beta}$ by any physical argument because $\tilde{\beta}$ is an off-diagonal matrix element of the field operator $\hat{\beta}$ according to (2.7) and therefore is not directly observable. However, the definition of $\tilde{\beta}$ (2.5), completely determines it.

The uniqueness of $\tilde{\beta}$ is easily seen at lowest order of the weak-field approximation. For small B , $Z[B, J]$ is of $O(B^2)$,

$$Z[B, 0] = -\frac{1}{2} B_i \left(\frac{1}{D} \right)_{ij} B_j + O(J^\dagger J) + O(J^\dagger J B) + O(B^3), \quad (2.9)$$

where $(1/D)_{ij} = (1/D)_{ji}$ contains the contribution of the β self-energy graphs. In this case, (2.5) leads to the following definition of $\tilde{\beta}$:

$$\tilde{\beta}_i = \left(\frac{1}{D} \right)_{ij} B_j + O(J^\dagger J) + O(B^2). \quad (2.10)$$

From (2.4) and the above, we find

$$S_{eff}[\tilde{\beta}, 0] = \frac{1}{2} \tilde{\beta}_i D_{ij} \tilde{\beta}_j + O(J^\dagger J \tilde{\beta}) + O(\tilde{\beta}^3).$$

The equation (2.8) translates into

$$D_{ij} \tilde{\beta}_j + \dots = B_i. \quad (2.11)$$

The general solution of the above equation is

$$\tilde{\beta}_i = \left(\frac{1}{D} \right)_{ij} B_j + \tilde{\beta}_i^0 + \dots \quad (2.12)$$

where $\frac{1}{D}$ is defined to be the same as the one that appear in Z of (2.9), and $\tilde{\beta}^0$ are zero modes defined by the following,

$$D_{ij} \tilde{\beta}_j^0 = 0.$$

According to (2.11), we have to exclude these $\tilde{\beta}^0$ from the solution (2.12).

The effective configuration given by (2.5), or equivalently (2.8) with zero modes subtracted, is complex. This is because S_{eff} has an imaginary part corresponding to the physical intermediate states or "cuts" in some of the graphs. For example, the graph illustrated in Fig. 1(a) has a cut C_1 corresponding to the one φ -pair state and thus gives an imaginary part to the D in (2.10) \sim (2.12). Therefore, $\tilde{\beta}_i$ in (2.11) is complex for nonzero real source B . This complexity of $\tilde{\beta}$ is in no contradiction with equation (2.7): Because of the nonzero B , the configuration of the β -field is excited out of the initial vacuum and subsequently φ -pairs are created. Therefore, $|0+\rangle$ is not the same state as $|0-\rangle^*$.

The effective configuration $\tilde{\beta}$ given by (2.10) is not retarded. In models with time-translational invariance, we can write (2.11) as follows;

$$\tilde{\beta}(x) = \int d^4x' \int d^4p G(p) e^{-i\varphi(x-x')} B(x') + O(B^2), \quad (2.13)$$

where we used the diagonal metric $(+---)$ and omitted indices. On the physical sheet of the complex p^0 -plane, $G(p)$ is analytic except for cuts on real axis corresponding to φ -pair creation. On the other hand, the imaginary part of $D(p)$ in (2.13) is always negative because the imaginary part of D is positive to insure

* The absence of zero modes in $\tilde{\beta}$ can also be understood in the following manner. If $B = 0$, nothing happens in the initial vacuum. Thus $|0+\rangle$ is proportional to $|0-\rangle$ and (2.7) gives $\tilde{\beta}_i = 0$.

the positivity of probabilities. Therefore, (2.13) can be written as

$$\tilde{\beta}(x) = \int d^4x' \int d^3p \int_C dp^0 G(p) e^{-ip(x-x')} B(x') + O(B^2) \quad (2.14)$$

where the contour C runs beneath the cut for $p_0 < 0$ and above the cut for $p^0 > 0$, as is illustrated in Fig. 2. Because of this contour, the propagator $1/D$ has an advanced part. For $t < t'$, the contour C can be deformed in the upper half-plane of p^0 to the contour C' . Thus, the discontinuity of the analytic function $G(p)$ on the negative real axis contributes to the advanced part of $1/D$. Since there are no zero-modes present to cancel this advanced part, $\tilde{\beta}$ has an advanced part, i.e., the effective configuration $\tilde{\beta}$ is not causal. The real configuration should not have this property.

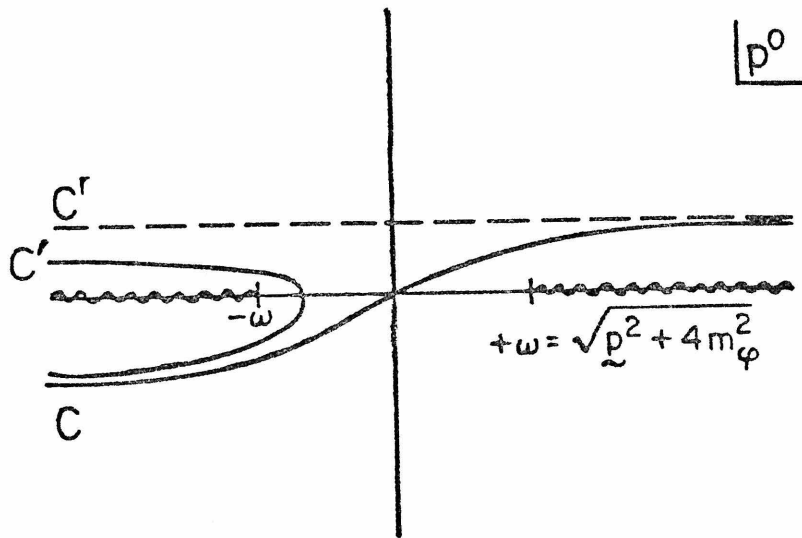


Figure 2: The analytic structure of $F(p)$ in (2.14) on the physical sheet of complex p^0 -plane. Since the β -configuration is unstable, the on-shell poles are on the unphysical sheet. The line C is the contour for $1/D$ in (2.14) and the line C^r is the contour for $1/D^r$ in (4.9).

3. Transition Amplitudes and Their Unitarity

Since the action and the source terms are Hermitian, the unitarity of the S-matrix should be satisfied,

$$S^+S = 1. \quad (3.1)$$

When we calculate transition amplitudes in perturbation expansion, it is very important to verify this unitarity at each order. It also clarifies the correspondence between a certain order of calculation of $\tilde{\beta}$ and the physical processes which are taken into account.

We define the states $|i-\rangle$ as the states which have definite quantum numbers at $t = -\infty$,

$$Q^{(M)}(t=-\infty)|i-\rangle = q_i^{(M)}|i-\rangle \quad (3.2)$$

where (M) denotes a set of all the necessary quantum numbers. Similarly, the states $|i+\rangle$ are defined by

$$Q^{(M)}(t=+\infty)|i+\rangle = q_i^{(M)}|i+\rangle.$$

Since the S-matrix elements are written as

$$S_{ij} = \langle i+|j-\rangle,$$

(3.1) reduces to

$$\sum_i \langle j-|i+\rangle \langle i+|j'-\rangle = \delta_{jj'}. \quad (3.3)$$

In this section, we verify this relation at the lowest order of the coupling-constant expansion of S_{eff} for two cases, (i) both $|j-\rangle$ and $|j'-\rangle$ are the initial vacuum state $|0-\rangle$, and (ii) $|j-\rangle$ is $|0-\rangle$ and $|j'-\rangle$ is an initial state $|a,b-\rangle$ with a φ -pair of quantum numbers (a, b) . Note that $J = 0$ unless otherwise

specified.

(i) Here we have $\langle 0- | 0- \rangle = 1$.

The first term in the expansion (3.3) has the intermediate state $|0+\rangle$ and is therefore vacuum-to-vacuum transition probability,

$$|\langle 0+ | 0- \rangle|^2 = |e^{i(S[\tilde{\beta}, 0] - \tilde{\beta}_j B_j)}|^2 \equiv e^{-R}, \quad (3.4)$$

where R is given by

$$R \equiv 2\text{Im} \left[S[\tilde{\beta}, 0] - \tilde{\beta}_i B_i \right] = -\text{Im} \left[B_i \left[\frac{1}{D} \right]_{ij} B_j \right] = -\text{Im}(\tilde{\beta}_i^* D_{ij}^I \tilde{\beta}_j) = \tilde{\beta}_i^* D_{ij}^I \tilde{\beta}_j.$$

Here, D^I is the imaginary part of D ($D = D^R + iD^I$), which comes from the graph (a) of Fig. 1.

The next term is the transition probability from the initial vacuum $|0-\rangle$ to the one φ -pair final state $|a, b+\rangle$, where a denotes the set of quantum numbers for the particle and antiparticle, respectively. The reduction formula and (2.3) give

$$\begin{aligned} \langle a, b+ | 0- \rangle &= P_{ai} \bar{P}_{bj} \langle 0+ | T(\hat{\varphi}_i \hat{\varphi}_j^\dagger) | 0- \rangle \\ &= P_{ai} \bar{P}_{bj} \frac{i\delta}{\delta J_i^\dagger} \frac{i\delta}{\delta J_i} \langle 0+ | 0- \rangle_{\beta, J} \Big|_{J=0} \\ &= P_{ai} \bar{P}_{bj} \left[\frac{\delta Z[B, J]}{\delta J_i^\dagger} \frac{\delta Z[B, J]}{\delta J_j} + \frac{-i\delta^2 Z[B, J]}{\delta J_i^\dagger \delta J_j} \right] e^{iZ} \Big|_{J=0}. \end{aligned} \quad (3.5)$$

Here, P_{ai} projects φ_i to the $t = +\infty$ annihilation operator for a φ -particle of quantum number a , and \bar{P}_{bj} does similarly for a φ -antiparticle [5]. To evaluate (3.5), we start from the following relation,

$$\frac{\delta Z[B, J]}{\delta J_j} = \frac{\delta S_{eff}[\tilde{\beta}, J]}{\delta J_j} \quad (3.6)$$

obtained from (2.4) and (3.5). Note that on the l.h.s. B is kept constant against the differentiation whereas on the r.h.s. $\tilde{\beta}$ is. Since S_{eff} is of $O(JJ^\dagger)$ and higher as is illustrated in Fig. 1(d) and (e), the first term in the left most side of (3.5) for vanishing J . Differentiating (3.6) with respect to J_i^\dagger , we learn

$$\frac{\delta^2 Z[B, J]}{\delta J_i^\dagger \delta J_j} = \frac{\delta^2 S_{eff}[\tilde{\beta}, J]}{\delta J_i^\dagger \delta J_j} + \frac{\delta \tilde{\beta}_k[B, J]}{\delta J_i^\dagger} \frac{\delta^2 S_{eff}[\tilde{\beta}, J]}{\delta \tilde{\beta}_k \delta J_j}.$$

The second term of the r.h.s. of the above equation vanishes for $J = 0$, because from (2.11),

$$\frac{\delta \tilde{\beta}}{\delta J^\dagger} = O(J).$$

Therefore, we obtain

$$\langle a, b+ | 0- \rangle = P_{ai} \bar{P}_{bj} \left. \frac{-i \delta S_{eff}[\tilde{\beta}, J]}{\delta J_i^\dagger \delta J_j} \right|_{J=0} \langle 0+ | 0- \rangle.$$

The r.h.s. of the above is $O(\tilde{\beta})$ because of the contribution of the graph (e) of Fig.

1. We write that term as

$$\langle a, b+ | 0- \rangle = i F_{abm}^+ \tilde{\beta}_m \langle 0+ | 0- \rangle + \dots \quad (3.7)$$

Since the above depends only on the quantum numbers a and b , F^+ causes a Fourier transform with total four-momentum, p_t , of the pair on $\tilde{\beta}$ in x -space:

$$F^+ \propto \int d^4x e^{-ip_t x}.$$

In particular, the superscript F^+ denotes that the time component is transformed with the positive energy. The total one-pair creation probability P_1

is

$$P_1 \equiv \sum_{a,b} |\langle a,b+ | 0-\rangle|^2 = |iF_{abm}^+ \tilde{\beta}_k|^2 e^{-R} = \tilde{\beta}_k^* F_{abk}^- F_{abm}^+ \tilde{\beta}_m e^{-R}, \quad (3.8)$$

where F^- denotes the conjugate of F^+ , which causes the Fourier transform with a negative energy.

Since, in the small $\tilde{\beta}$ limit,

$$[\text{total pair creation probability}] = 1 - |\langle 0+ | 0-\rangle|^2 \sim P_1,$$

the following relation should be true,

$$\tilde{\beta}_k^* F_{abk}^- F_{abk}^+ \tilde{\beta}_k = R. \quad (3.9)$$

We prove as follows: First, note that

$$D_{kk}^I = \frac{1}{2} \left(F_{abk}^- F_{abk}^+ + F_{abk}^+ F_{abk}^- \right). \quad (3.10)$$

This form is explained by the fact that D depends only on the square of the external momentum. Furthermore, in the test-field approximation, i.e., if φ -pairs are created by an externally fixed (i.e., nondynamical) $\tilde{\beta}$, (3.9) follows from (2.10) because of the reality of $\tilde{\beta}$. In our dynamical case, however, (3.9) is not trivial because $\tilde{\beta}$ is complex; it is therefore necessary to use (2.11) as follows:

$$\begin{aligned} \text{l.h.s. of (3.9)} &= B \frac{1}{D^*} F^- F^+ \frac{1}{D} B \\ &= \sum_{n,m=0}^{\infty} (i)^{n-m} B \frac{1}{D^R} \left[D^I \frac{1}{D^R} \right]^n F^- F^+ \frac{1}{D^R} \left[D^I \frac{1}{D^R} \right]^m B \\ &= \frac{1}{2} \sum_{n,m} (i)^{n-m} B \frac{1}{D^R} \left[D^I \frac{1}{D^R} \right]^n \left(F^- F^+ + (-1)^{n-m} F^+ F^- \right) \\ &\quad \frac{1}{D^R} \left[D^I \frac{1}{D^R} \right]^m B \end{aligned}$$

$$\begin{aligned}
 &= \sum_{n-m=\text{even}} (i)^{n-m} B \frac{1}{D^R} \left[D^I \frac{1}{D^R} \right]^n D_I \frac{1}{D^R} \left[D^I \frac{1}{D^R} \right] B \\
 &= B \frac{1}{D^*} D^I \frac{1}{D} B = r.h.s. \text{ of (3.9)}
 \end{aligned}$$

where the indices have been omitted for simplicity. Thus, at this order, (3.8) leads to

$$P_1 = \text{Re}^{-R}.$$

In the similar way, it is easy to show that the total n -pair creation probability P_n is given by

$$P_n = \frac{R^n}{n!} e^{-R} + \dots \quad (3.11)$$

Here the first term corresponds to the totally incoherent production of n -pairs, which is illustrated in Fig. 3.

By summing only the incoherent multipair production probabilities, we obtain

$$\sum_n \frac{R^n}{n!} e^{-R} = 1 = \langle 0- | 0- \rangle.$$

That is, our calculation of S_{eff} and $\tilde{\beta}$ at the level of Fig. 1(a) is equivalent to counting only the incoherent production processes: Only when we extend our calculation to graphs which are cut into more than two pieces, we begin taking into account the coherent production processes*.

* When S_{eff} is calculated in the loop expansion, summation over all coherent terms of (3.11) becomes important for unitarity. In the charged pair creation model in a constant electric field, $\text{Im}(S_{eff})$ was calculated by Schwinger [7] in the proper time method. The author and Kobayashi [8] gave the coherent part of P_n and showed that the Schwinger's result is reproduced by using unitarity.

(ii) In this case: $\langle a, b- | 0- \rangle = 0$

For the calculation of the lowest order term, we note that

$$\langle 0+ | a, b- \rangle = i F_{abk}^- \tilde{\beta}_k \langle 0+ | 0- \rangle.$$

This leads to

$$\langle a, b- | 0+ \rangle \langle 0+ | 0- \rangle = -i F_{abk}^+ \tilde{\beta}_k^* e^{-R}. \quad (3.12)$$

Similarly, the next term is obtained as follows,

$$\begin{aligned} & \sum_{a'b'} \langle a, b- | a'b'+ \rangle \langle a'b'+ | 0- \rangle \\ &= (i F_{abk}^+ \tilde{\beta}_k - i F_{abk}^+ \left[\frac{-i}{D^*} \right]_{kk'} F_{a'b'k}^- F_{a'b'l}^+ \tilde{\beta}_l - i F_{abk}^+ \tilde{\beta}_k^* R) e^{-R} \end{aligned} \quad (3.13)$$

where we used (3.9). The graphs corresponding to (3.12) and (3.13) are illustrated in Fig. 4(a) and 4(b), respectively. The $(n+1)th$ term, i.e., the term with n -pairs "+" intermediate state, has the following incoherent parts;

$$\left[(I+II) \frac{R^{n-1}}{(n-1)!} + III \frac{R^n}{n!} \right] e^{-R}$$

where I , II and III represent the 1st, 2nd and 3rd terms of (3.13), respectively.

Summing over these incoherent parts, we obtain

$$\langle a, b- | 0- \rangle = -i F^+ \tilde{\beta}^* + i F^+ \tilde{\beta} - i F^+ \frac{-i}{D^*} F^- F^+ \tilde{\beta}, \quad (3.14)$$

where we have omitted trivial indices.

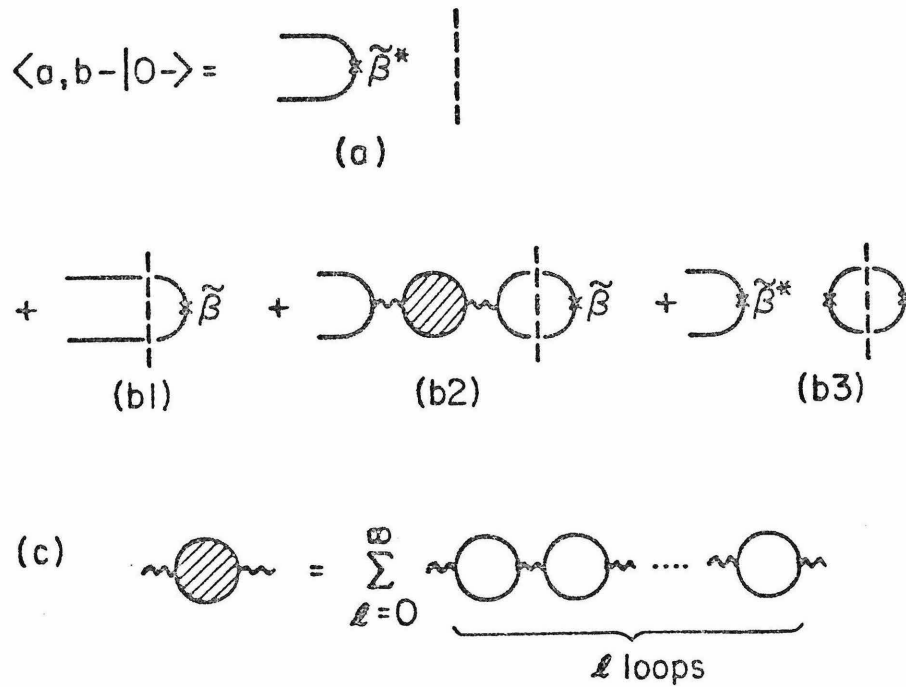


Figure 4: The matrix element $\langle a, b | 0 \rangle$. The graph (a) and (b1) ~ (b3) represent (3.12) and the three terms of (3.13), respectively. The content of the "dressed" propagator $1/D$ is illustrated in (c).

When the β -field is not dynamical and $\tilde{\beta}$ is merely a given real function as it is in the test-field approximation, the r.h.s. of (3.14) is zero. Since there are no virtual β -quanta, the third term of (3.14) does not exist in such models. The first and second terms cancel each other simply because $\tilde{\beta}$ is a real function.

In our dynamical case, the r.h.s. of (3.14) is verified to be zero with the help of the energy conservation rule,

$$\mathbf{F}^\pm \frac{1}{D} \mathbf{F}^\pm = 0. \quad (3.15)$$

Adding

$$0 = -i\mathbf{F}^+ \frac{-i}{D^*} \mathbf{F}^+ \mathbf{F}^- \tilde{\beta}$$

to the third term of r.h.s. of (3.14), we obtain

$$\begin{aligned} -i\mathbf{F}^+ \frac{-i}{D^*} \mathbf{F}^- \mathbf{F}^+ \tilde{\beta} &= i\mathbf{F}^+ \frac{i}{D^*} 2D^I \tilde{\beta} = i\mathbf{F}^+ \frac{1}{D^*} (D - D^*) \frac{1}{D} B \\ &= i\mathbf{F}^+ (\tilde{\beta}^* - \tilde{\beta}), \end{aligned} \quad (3.16)$$

where we used (2.11) and (3.10). Therefore, (3.14) is equal to zero.

The other unitarity relations can be verified in a similar way by using the basic relations (3.9) and (3.16). It is important to note that, in contrast to the test-field approximation, unitarity does not hold for arbitrary complex functions $\tilde{\beta}$. The effective action $\tilde{\beta}$ has to satisfy (2.11) with the real source B for (3.9) and (3.16). And for (2.11), it is necessary that $D\tilde{\beta}$ be a real function. Therefore, $\tilde{\beta}$ cannot be any arbitrary function.

So far, we have limited ourselves to study the lowest nontrivial order of the coupling expansion: Only the contributions of the graphs (a), (e) and (d) of Fig. 1 to the S_{eff} have been taken into account. However, the discussion of unitarity given in this section can be easily extended to include any graphs which contribute to $O(\tilde{\beta}^2 \cdot J^0)$ of S_{eff} such as graph (b) of Fig. 1.

4. The Real Configuration

In previous sections, we observed that matrix elements are given by the effective configuration $\tilde{\beta}$ defined as the Schwinger average (2.7) of the β -field operator $\hat{\beta}$,

$$\tilde{\beta}_i = \frac{\langle 0+ | \hat{\beta}_i | 0- \rangle}{\langle 0+ | 0- \rangle}. \quad (2.7)$$

For nonvanishing B , the initial vacuum state $|0-\rangle$ has φ -pairs as $t \rightarrow +\infty$ and therefore represents the different states $|0+\rangle$; $|0-\rangle$ is not proportional to $|0+\rangle$. Because of this reason, $\tilde{\beta}$ is complex and is not an directly observable quantity itself. The real configuration β^r , the configuration of the β -field that we observe, is defined as follows;

$$\beta_i^r \equiv \langle 0- | \hat{\beta}_i | 0- \rangle. \quad (4.1)$$

This quantity is calculable in the following form

$$\beta_i^r = \sum_j \langle 0- | j+ \rangle \langle j+ | \hat{\beta}_i | 0- \rangle, \quad (4.2)$$

in the framework of the effective action method described so far. As we did in the previous section, we first deal with (4.1) at the level of Fig. 1(a).

It is easy to find the first term, $j = 0$:

$$\langle 0- | 0+ \rangle \langle 0+ | \hat{\beta}_i | 0- \rangle = \tilde{\beta}_i e^{-R}. \quad (4.3)$$

This is represented graphically in Fig. 5(a). For the next term, we need a new matrix element $\langle a, b+ | \hat{\beta}_i | 0- \rangle$, which is calculated as follows,

$$\begin{aligned} \langle a, b+ | \hat{\beta}_i | 0- \rangle &= i \frac{\delta}{\delta B_i} \langle a, b+ | 0- \rangle \\ &= i \frac{\delta}{\delta B_i} \left[i F_{abk}^t \tilde{\beta}_k \langle 0+ | 0- \rangle \right] \end{aligned}$$

$$= \left[i F_{abk}^{\dagger} \frac{i \delta \tilde{\beta}_k}{\delta B_i} + i F_{abk}^{\dagger} \tilde{\beta}_k \tilde{\beta}_i \right] \langle 0+ | 0- \rangle$$

and (3.7) and (3.9) lead to

$$\sum_{a,b} \langle 0- | a,b+ \rangle \langle a,b+ | \hat{\beta}_i | 0- \rangle = \left[\tilde{\beta}_k \cdot F_{abk}^{-} \cdot F_{abk}^{\dagger} \frac{i \delta \tilde{\beta}_k}{\delta B_i} + R \tilde{\beta}_i \right] e^{-R}. \quad (4.4)$$

Here, $\delta \tilde{\beta} / \delta B$ is the full propagator of the β -field because, from (2.5), it is just the second derivative of Z by B . At the order we are working, (2.11) gives

$$\frac{i \delta \tilde{\beta}_k}{\delta B_i} = \left(\frac{i}{D} \right)_{ki}.$$

Therefore, (4.4) can be represented as in Fig. 5(b). The second term of (4.4) partially cancels the factor e^{-R} of (4.3) as the third term in (3.13) did for (3.12). The incoherent part of the $(n+1)$ th term is

$$\left[\tilde{\beta} F^{-} F^{+} \frac{i}{D} \cdot \frac{R^{n-1}}{(n-1)!} + \frac{R^n}{n!} \tilde{\beta} \right] e^{-R},$$

as is illustrated in Fig. 5(c). Therefore, by summing all these incoherent higher order terms, we obtain

$$\beta_i^{\Gamma} = \tilde{\beta}_i + \left(\frac{i}{D} \right)_{ki} F_{abk}^{\dagger} F_{abk}^{-} \tilde{\beta}_k^*. \quad (4.5)$$

To verify the reality of r.h.s. of (4.5), we operate F 's on (4.5) [5]:

$$F^{+} \beta^{\Gamma} = F^{+} \left[\tilde{\beta} + \frac{i}{D} F^{+} F^{-} \tilde{\beta}^* \right] = F^{+} \tilde{\beta}. \quad (4.6a)$$

$$F^{-} \beta^{\Gamma} = F^{-} \left[\tilde{\beta} + \frac{i}{D} (F^{+} F^{-} + F^{-} F^{+}) \tilde{\beta}^* \right] = F^{-} \left[\frac{1}{D} + \frac{1}{D} (D - D^*) \frac{1}{D^*} \right] B = F^{-} \tilde{\beta}^*, \quad (4.6b)$$

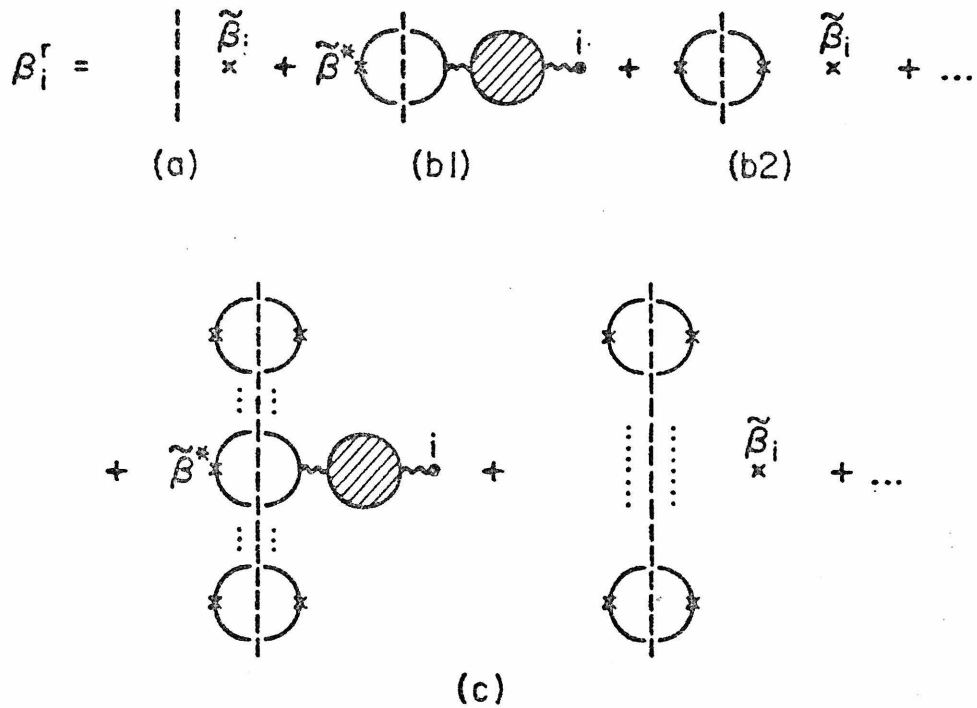


Figure 5: The real configuration β_i^r . The graph (a), (b1) and (b2) represent (4.3) and the two terms of (4.4), respectively. In the third graph, the isolated broken loops correspond to R . The $(n+1)$ th term is illustrated in (c).

where we have used the energy conservation law (3.15). From the above, we find

$$\mathbf{F}^+(\beta^{r*}) = (\mathbf{F}^-\beta^r)^* = (\mathbf{F}^-\tilde{\beta}^*)^* = \mathbf{F}^+\tilde{\beta} = \mathbf{F}^+\beta^r,$$

and similarly,

$$\mathbf{F}^-(\beta^{r*}) = \mathbf{F}^-\beta^r.$$

Therefore, β^r given by (4.5) is real.

In terms of B , (4.5) can be expressed as follows;

$$\beta^r = \left(\frac{1}{D} + \frac{i}{D} \mathbf{F}^+ \mathbf{F}^- \frac{1}{D^*} \right) B = \frac{1}{D} \left(D^* + i \mathbf{F}^+ \mathbf{F}^- \right) \frac{1}{D^*} B = \frac{1}{D^r} B, \quad (4.7)$$

where

$$D^r = D - i \mathbf{F}^+ \mathbf{F}^- = D^R + \frac{i}{2} (-\mathbf{F}^+ \mathbf{F}^- + \mathbf{F}^- \mathbf{F}^+). \quad (4.8)$$

The last equality of (4.7) can be proven as follows: First, we define

$$D^\pm = \frac{i}{2} \mathbf{F}^\mp \mathbf{F}^\pm,$$

respectively. Expanding $1/D$ and $1/D^*$ in powers of D^+ and D^- , we get

$$\begin{aligned} \frac{1}{D} D^r \frac{1}{D^*} &= \sum_{n=0}^{\infty} \sum_{m=0}^{\infty} \frac{(-1)^n}{D^R} \left[(D^+ + D^-) \frac{1}{D^R} \right]^n (D^R - D^+ + D^-) \frac{1}{D^R} \left[(D^+ + D^-) \frac{1}{D^R} \right]^m \\ &= \sum_n \sum_m \frac{(-1)^n}{D^R} \left\{ \left[D^+ \frac{1}{D^R} \right]^{n+m} + \left[D^- \frac{1}{D^R} \right]^{n+m} - \left[D^+ \frac{1}{D^R} \right]^{n+m+1} + \left[D^- \frac{1}{D^R} \right]^{n+m+1} \right\} \end{aligned}$$

where we have used (3.15). Changing the index (n, m) to $(N = n + m, n)$, we find

$$\frac{1}{D} D^r \frac{1}{D^*} = \sum_{N=0}^{\infty} \frac{1}{D^R} \left\{ \left[D^+ \frac{1}{D^R} \right]^N (C_N - C_{N-1}) + \left[D^- \frac{1}{D^R} \right]^N (C_N + C_{N-1}) \right\}$$

$$\begin{aligned}
 &= \sum_{N=0}^{\infty} \frac{1}{D^R} \left\{ (-1)^N \left[D^+ \frac{1}{D^R} \right]^N + \left[D^- \frac{1}{D^R} \right]^N \right\} \\
 &= \sum_{N=0}^{\infty} \frac{1}{D^R} \left[(-D^+ + D^-) \frac{1}{D^R} \right]^N = \frac{1}{D^R + D^+ - D^-}
 \end{aligned}$$

where

$$C_N \equiv \sum_{n=0}^N (-1)^n = \frac{1}{2}(1+(-1)^N).$$

The causal structure of β^r is manifest in (4.7). The only difference between (2.11) and (4.7) lies in the sign of D^- , which is the negative-energy imaginary part of D^* . Thus (4.7) can be expressed in terms of the same $F(p)$ defined in (2.14);

$$\beta^r(x) = \int d^4x' \int d^3p \int_{C^r} dp^0 G(p) e^{-i\varphi(x-x')} B(x'). \quad (4.9)$$

The new contour C^r has to run above the cut for both $p^0 > 0$ and $p^0 < 0$, reflecting the difference of sign in D^- (see Fig. 6). Comparing the contours C and C^r , we notice that the second term in (4.5) corresponds to the integration of the same integrand as in the r.h.s. of (4.9) along the contour C' in Fig. 2. For $t < t'$, the contour closes in the upper half plane where no singularities exist. Therefore, the "propagator" $1/D^r$ is retarded, and $\beta^r(x)$ has no advanced part, that is, β^r becomes nonzero only after the source B has. This causal property of β^r agrees with the physical picture that $|0-\rangle$ is the vacuum not only in φ -sector but also in β -sector before the source B attains a nonzero value. The real configuration β^r is zero initially and gets excited by the source B .

* This difference is also understood from (4.6): If one defines $1/D^r$ as $\beta^r = \frac{1}{D^r} B$, (4.6b) implies that the imaginary part of $1/D^r$ for negative energy has different sign from that of $1/D^*$, while it is not so for positive energy. This argument completely determines $1/D^r$.

Since we gave the relation between the effective configuration $\tilde{\beta}$ and the real configuration β^r , the transition amplitudes, which are given in terms of $\tilde{\beta}$, can also be given in terms of β^r . For example, by substituting (4.6) into (3.9), we find that the vacuum-to-vacuum transition probability e^{-R} is obtained from β^r by

$$R = \beta^r F^- F^+ \beta^r. \quad (4.10)$$

Similarly, the one pair creation amplitude (2.7) is

$$\langle a, b+ | 0- \rangle = i F_{abm}^+ \beta_m^r e^{-R}. \quad (4.11)$$

The inverse of (4.5) is also useful:

$$\tilde{\beta} = \frac{1}{D} B = \frac{1}{D} D^r \beta^r = \beta^r - \frac{i}{D} F^+ F^- \beta^r. \quad (4.12)$$

From this formula, the one-pair annihilation probability is obtained as follows:

$$\langle 0+ | a, b- \rangle = i F_{abm}^- \tilde{\beta}_m = i F_{abm}^- \left[\beta^r - \frac{i}{D} 2D_I \beta^r \right]_m = i F_{abm}^- \left[\frac{1}{D} D^* \beta^r \right]_m. \quad (4.13)$$

It should be noted that, as is illustrated in the above examples, all the matrix elements are calculated from the physical quantity β^r .

In this section, we worked at the order of the graph of Fig. 1. However, any $O(\tilde{\beta}^2)$ contribution to S_{eff} can be easily included in the results. In particular, the causal property of the β^r remains unchanged: The real configuration β^r is always retarded. The Green's function $1/D$ has various cuts on the real axis of complex p_0 -plane, while the retarded Green's function $1/D^r$ is always obtained by shifting the integration contour to the upper half-plane.

5. Conclusion and Discussion

We have developed the effective action method to deal with unstable configurations by using a two field model, where we have a β -field whose configurations are observed and a φ -field whose pairs are created. At the lowest nontrivial order of the weak β -field approximation, i.e., at $O(\beta^2)$ of the effective action S_{eff} , the unitarity conditions among the φ -pair creation and the φ -pair annihilation amplitudes are verified. Because of the dynamical property of the β -field, the effective configuration $\tilde{\beta}$, in terms of which the transition amplitudes are expressed, is complex and made unitarity nontrivial. By the same reason, however, β -quanta can appear as internal lines of the Feynman graphs and are shown to save unitarity.

Furthermore, we derived the equations relating the real configuration β^r and the effective configuration $\tilde{\beta}$, which were used to show that β^r is causal as we expected on physical grounds. Using results of the unitarity discussion, we were able to sum the higher-order incoherent terms in the expansion of β^r to obtain (4.5). Then (4.5) was converted into (4.6) and (4.7). The equation (4.7) has a consequence that the real configuration β^r is retarded relative to the source B . This agrees with the physical picture that our initial state $|0\rangle$ is initially the vacuum state, and the real configuration β^r is excited by the source B .

In higher orders of the weak-field approximation, β^r is related to $\tilde{\beta}$ as

$$\beta^r = \tilde{\beta} + [\text{connected terms such as Fig. 5(b 1)}], \quad (5.1)$$

as the extension of (4.5). In general, the connected terms in the above are nonlinear both in $\tilde{\beta}$ and $\tilde{\beta}^*$. For example, when $O(\tilde{\beta}^3)$ of S_{eff} is taken into account, the connected terms in (5.1) are of $O(\tilde{\beta}^2) + O(\tilde{\beta}\tilde{\beta}^*) + O(\tilde{\beta}^{*2})$. Because of this nonlinearity, the simple relations like (4.6a) and (4.6b) would not hold at higher orders*. However, on physical grounds, we expect that the causal structure of

* A partial discussion at this order is given in Ref. [9].

β^r does not change. β^r should be nonzero only after the source B has. Thus, the expression (4.7) of β^r in terms of B is expected to be generalized as follows;

$$\beta^r = \sum_n \int d^4x_1 \dots d^4x_n G_n^r(x; x_1 \dots x_n) B(x_1) \dots B(x_n), \quad (5.2)$$

where G_n^r 's are real, retarded Green's functions,

$$G_n^r(x; x_1 \dots x_n) = 0 \quad \text{if } t < \text{any } t_i.$$

The G_n^r is obtained by the $(N+1)$ -point connected Green's function G_n by deforming the integration contour: The first term $\tilde{\beta}$ on the r.h.s. of (5.1) is given by

$$\tilde{\beta}(x) = \sum_n \int d^4x_1 \dots d^4x_n G_n(x; x_1 \dots x_n) B(x_1) \dots B(x_n), \quad (5.3)$$

and the connected terms in (5.1) then add the discontinuity to G_n 's so that the sum becomes the retarded Green's function G_n^r 's. For practical purposes, the generalization of the equation (4.8) for β^r would be more useful than (5.2) because the source B is implicit in most actual applications*.

Throughout this chapter, we have assumed that the field configuration is totally unstable, i.e., $m_\beta^2 > 4m_\phi^2$, where m_β denotes the mass of a β -quantum. However, the effective action method as developed here can also be applied to the case where $m_\beta^2 < 4m_\phi^2$, when only a part of the configuration decays. In such a case, $G(p)$ in (2.14) has on-shell poles $p_0 = \pm\sqrt{\mathbf{p}^2 + m_\beta^2}$ on the physical sheet Fig. 2 of complex p_0 -plane. These poles cause further complexity of $\tilde{\beta}$. In the expansion (4.2) of β^r , however, we have an extra contribution from + states which have some configuration left over, which makes β^r real and causal again.

* The proof of (5.2) was recently given by Sonoda [10].

Appendix. The Operator Field Equations and the Real Configuration

Relation (4.5) between the real configuration β^r and the effective configuration $\tilde{\beta}$ is consistent with the operator field equations. The purpose of this appendix is to reproduce (4.5) from the operator field equations using naive arguments.

We write the bare action $S[\beta, \varphi]$ explicitly as follows;

$$S[\beta, \varphi] = \frac{1}{2} \beta_i D_{ij}^0 \beta_j + \varphi_i^\dagger d_{ij} \varphi_j + g_{ik} \beta_i \varphi_l^\dagger \varphi_k. \quad (\text{A.1})$$

Then, the β -field operator $\hat{\beta}$ and the φ -field operator $\hat{\varphi}$ satisfy the following;

$$D_{ij}^0 \hat{\beta}_j + g_{ik} \hat{\varphi}_l^\dagger \hat{\varphi}_k = B_i, \quad (\text{A.2})$$

$$d_{ij} \hat{\varphi}_j + g_{ik} \hat{\beta}_l \hat{\varphi}_k = 0, \quad (\text{A.3})$$

where we have neglected the source J for simplicity. First, we take the matrix element of (A.2) between $\langle 0+ |$ and $| 0-\rangle$.

$$D_{ij}^0 \langle 0+ | \hat{\beta}_j | 0-\rangle + g_{ik} \langle 0+ | \hat{\varphi}_l^\dagger \hat{\varphi}_k | 0-\rangle = B_i \langle 0+ | 0-\rangle. \quad (\text{A.4})$$

In the above, the second term of the l.h.s. is a local product and is well-defined as an equal time limit of the T -product. Therefore, we substitute $\langle 0+ | \hat{\varphi}_l^\dagger \hat{\varphi}_k | 0-\rangle$ by $\langle 0+ | T(\hat{\varphi}_l^\dagger \hat{\varphi}_k) | 0-\rangle$, which satisfies

$$\langle 0+ | T(\hat{\varphi}_l^\dagger \hat{\varphi}_k) | 0-\rangle = \langle 0+ | T \left[\frac{-i}{d+g\hat{\beta}} \right]_{lk} | 0-\rangle. \quad (\text{A.5})$$

This relation is most easily obtained in the path integral formalism as follows:

For the action (A.1), the $[d\varphi][d\varphi^\dagger]$ integration in (2.3) can be done to yield

$$e^{iZ[B, J]} = \int [d\beta] \frac{\det d}{\det(d+g\beta)} e^{i\left\{ \beta D^0 \beta - J^\dagger \frac{1}{d+g\beta} J \right\}}.$$

Therefore,

$$\begin{aligned}
 \langle 0+ | T(\hat{\varphi}_i^\dagger \hat{\varphi}_k) | 0-\rangle &= \frac{i\delta}{\delta J_i} \frac{i\delta}{\delta J_k^\dagger} e^{iZ[B,J]} \Big|_{J=0} \\
 &= \int [d\beta] \left[\frac{-i}{d+g\beta} \right]_{ik} \frac{\det d}{\det(d+g\beta)} e^{i(\dots)} \\
 &= \langle 0+ | \left[\frac{-i}{d+g\hat{\beta}} \right]_{ik} | 0-\rangle.
 \end{aligned}$$

In the expansion of (A.5) in terms of the coupling g , $g_{ik} \times$ [the first term], which is represented by a tadpole graph, vanishes corresponding to the fact that we assumed no $O(B)$ term in Z of (2.10). Therefore, (A.4) reduces to

$$\left[D^{0+ig} \frac{1}{d} g \frac{1}{d} \right]_{ij} \frac{\langle 0+ | \hat{\beta}_j | 0-\rangle}{\langle 0+ | 0-\rangle} + \dots = B_j. \quad (\text{A.6})$$

Here we defined

$$\left[g \frac{1}{d} g \frac{1}{d} \right]_{ij} \equiv g_{ik} \left[\frac{1}{d} \right]_{km} g_{jnm} \left[\frac{1}{d} \right]_{nk}.$$

Equation (4.6) is equivalent to (2.12) at the order of the graph (a) of Fig. 1.

To obtain (4.5) from the operator field equations, we take the expectation value of (A.2) in the initial vacuum state, $|0-\rangle$:

$$D_{ij}^0 \langle 0- | \hat{\beta}_j | 0-\rangle + g_{ik} \langle 0- | T(\hat{\varphi}_i^\dagger \hat{\varphi}_k) | 0-\rangle = B_i. \quad (\text{A.7})$$

We can calculate the second term of the l.h.s. of (A.6) by inserting $1 = \sum_n |n+\rangle \langle n+|$. Then, the first term of the series,

$$g_{ik} \sum_j \langle 0- | j+\rangle \langle j+ | T(\hat{\varphi}_i^\dagger \hat{\varphi}_k) | 0-\rangle,$$

is given by

$$\begin{aligned}
 g_{uk} \langle 0- | 0+ \rangle \langle 0+ | T \left[\frac{-i}{d+g\hat{\beta}} \right]_{lk} | 0- \rangle &= g_{uk} \langle 0- | 0+ \rangle \left[i \frac{1}{d} g \langle 0+ | \hat{\beta} | 0- \rangle \frac{1}{d} \right]_{lk} + \dots \\
 &= g_{uk} \left[i \frac{1}{d} g \tilde{\beta} \frac{1}{d} \right]_{lk} e^{-R}. \tag{A.8}
 \end{aligned}$$

The next term, $j = (a, b)$, yields the following:

$$\begin{aligned}
 g_{uk} \sum_{a,b} \langle 0- | a, b+ \rangle \langle a, b+ | T(\hat{\varphi}_i^\dagger \hat{\varphi}_k) | 0- \rangle \\
 = -i \tilde{\beta}_m^* F_{abm}^- F_{abi}^+ - i \tilde{\beta}_m^* F_{abm}^- F_{abj}^+ \left[\frac{1}{D} \right]_{jn} \left[-ig \frac{1}{d} g \frac{1}{d} \right]_{ni} + R g_{uk} \left[i \frac{1}{d} g \tilde{\beta} \frac{1}{d} \right]_{lk} \tag{A.9}
 \end{aligned}$$

where (3.9) has been used. The graphs that represent (A.7) and (A.8) are illustrated in (a) and (b) of Fig. 6, respectively. By summing all the incoherent contributions of multipair intermediate states, we obtain

$$\begin{aligned}
 g_{uk} \langle 0- | T(\hat{\varphi}_i^\dagger \hat{\varphi}_k) | 0- \rangle &= -i \tilde{\beta}_m^* F_{abm}^- F_{abi}^+ - i \tilde{\beta}_m^* F_{abm}^- F_{abj}^+ \left[\frac{1}{D} \right]_{jm} \left[-ig \frac{1}{d} g \frac{1}{d} \right]_{ni} \\
 &\quad + ig_{uk} \left[\frac{1}{d} g \tilde{\beta} \frac{1}{d} \right]_{lk}.
 \end{aligned}$$

Therefore, (A.6) reduces to

$$D^0 \beta^r - i F^+ F^- \tilde{\beta}^* - i \left[g \frac{1}{d} g \frac{1}{d} \right] \frac{1}{D} (-i F^+ F^-) \tilde{\beta}^* + i \left[g \frac{1}{d} g \frac{1}{d} \right] \tilde{\beta} = B. \tag{A.10}$$

Since, at this order,

$$D \equiv D^0 + ig \frac{1}{d} g \frac{1}{d},$$

the second and the third terms of the l.h.s. of (A.10) combine into

$$g_{i||k} \langle 0- | T(\hat{\varphi}_i^\dagger \hat{\varphi}_k) | 0-\rangle = \begin{array}{c} | \\ \tilde{B}^* \circlearrowleft i \end{array}$$

(a)

$$\tilde{B}^* \circlearrowleft i + \begin{array}{c} | \\ \circlearrowleft \text{---} \text{---} \text{---} \circlearrowleft i \end{array} + \begin{array}{c} | \\ \circlearrowleft \tilde{B}^* \circlearrowleft i \end{array} + \dots$$

(b)

Figure 6: The matrix element $g_{uk} \langle 0- | T(\hat{\varphi}_i^\dagger \hat{\varphi}_k) | 0-\rangle$. The graphs (a) and (b) correspond to (A.7) and (A.8), respectively.

$$D_0 \frac{1}{D} (-i\mathbf{F}^+\mathbf{F}^-) \tilde{\beta}^*.$$

By substituting (A.6), or its equivalent (2.12), $D\tilde{\beta} = B$ into the r.h.s. of (A.10), we obtain

$$D^0\beta^r = D^0\tilde{\beta} + D_0 \frac{1}{D} (-i\mathbf{F}^+\mathbf{F}^-) \tilde{\beta}^*.$$

The general solution to the above is

$$\beta^r = \tilde{\beta} - i \frac{1}{D} \mathbf{F}^+\mathbf{F}^- \tilde{\beta}^* + [\text{zero modes of } D^0]. \quad (\text{A.11})$$

The zero modes in the above are excluded by physical arguments: The first two terms of (A.11) are, as is shown in Section IV, retarded, while, in general, the zero modes span all space-time. Therefore, if the zero modes exist in (A.11), β^r has always an advanced part. However, it is not allowed because the state $|0\rangle$ is the vacuum state before the source \tilde{B} becomes nonzero. Thus, the zero modes are excluded from (A.11) to yield (4.5).

References for Chapter II

- [1] J. Schwinger, Proc. Nat. Acad. Sci. 37 (1951) 452, 455; E. S. Abers and B. W. Lee, Phys. Rep. 9C (1973) 1; B. S. DeWitt, "Quantum Gravity: the New Synthesis" in "General Gravity, an Einstein Centenary Survey," (Edited by S. W. Hawking and W. Israel, Cambridge University Press, London, 1979).
- [2] M. V. Fischetti, J. B. Hartle and B. L. Hu, Phys. Rev. D20 (1979) 1757.
- [3] J. B. Hartle and B. L. Hu, Phys. Rev. D20 (1979) 1772.
- [4] J. B. Hartle and B. L. Hu, Phys. Rev. D21 (1980) 2756; J. B. Hartle, Phys. Rev. D22 (1980) 2091; J. B. Hartle, "Particle Production and Dynamics in the Early Universe," UCSB preprint TH-50 (1980).
- [5] H. Aoyama, Phys. Lett. 107B (1981) 39.
- [6] H. Aoyama, Caltech preprint, CALT-68-900.
- [7] J. Schwinger, Phys. Rev. 82 (1951) 664.
- [8] H. Aoyama and M. Kobayashi, Prog. of Theor. Phys. 64 (1980) 1045.
- [9] H. Aoyama, Soryushiron Kenkyu (Kyoto) 63 (1981) 239.
- [10] H. Sonoda, Private communication.

III. Anisotropy Dissipation Model of the Early Universe

1. Hartle and Hu's Model

One of the possible mechanisms for dissipation of an anisotropy in the early universe is creation of conformally invariant particle pairs. If a field Φ is coupled to gravity in the conformally invariant manner, Φ -pairs are not created in an isotropically expanding universe [1]. Thus, an anisotropic universe is expected to be driven to be isotropic by creation of Φ -pairs. This mechanism was studied, and shown to work, by several people by using semi-classical methods [2]. These methods, however, had difficulties. The total pair creation probability diverged as one approached the initial singularity, indicating that the semi-classical methods were not applicable near the singularity. To avoid this difficulty of traditional methods, Hartle, Hu, and others [3~7] applied the effective action method to this problem. They showed that the singularity of the production probability is removed by the quantum correction, which can be treated systematically by the effective action method.

In terms of the effective action method studied in chapter II, they calculated the effective configuration $\tilde{g}_{\mu\nu}$, which they called the effective geometry, of the quantum metric operator $\hat{g}_{\mu\nu}$. The given numerical solutions $\tilde{g}_{\mu\nu}$ have, as expected, an imaginary part. The purpose of this chapter is to study the relation between the effective geometry and the real configuration $g_{\mu\nu}^r$, which we call the real geometry in Hartle and Hu's model. This section outlines the work done by Hartle and Hu in a manner suitable for further analysis in the next section.

The action at the tree level is

$$S = \int d^4x \sqrt{-g} \left[\frac{1}{16\pi G} R - \frac{1}{2} \left(g^{\mu\nu} \partial_\mu \Phi \partial_\nu \Phi + \frac{R}{6} \Phi^2 \right) + [\text{radiation term}] \right] \quad (1.1)$$

where φ is the real scalar field, and the classical radiation is put in to give the usual expanding universe at the tree level. Assuming spatial homogeneity, we write the metric as

$$dS^2 = a^2(\eta) \left[d\eta^2 - \sum_{i,j=1}^3 \left(e^{2\beta(\eta)} \right)_{ij} dx^i dx^j \right] \quad (1.2)$$

where the traceless matrix $\beta_{ij}(\eta)$ represents the anisotropy in the expansion rates of the universe. The action in terms of this metric is

$$S = S_{\text{gravity}}[a, \beta] + \int d\eta d^3x \left[\frac{1}{2} \left(\left(\frac{\partial \varphi}{\partial \eta} \right)^2 - \sum_{i=1}^3 \left(\frac{\partial \varphi}{\partial x^i} \right)^2 \right) + \varphi F[\beta] \varphi \right] \quad (1.3)$$

$$F[\beta] = \sum_{i,j=1}^3 \frac{\partial}{\partial x^i} \beta_{ij}(\eta) \frac{\partial}{\partial x^j} + O(\beta^2), \quad (1.4)$$

where

$$\varphi(x) \equiv a(x) \Phi(x).$$

The gravitational action in (1.3) is given by [4],

$$S_{\text{gravity}}[\alpha, \beta] = \frac{V}{16\pi G} \int d\eta \left(-6(\alpha')^2 + a^2 \beta'_{ij} \beta'_{ij} + O(\beta^3) \right), \quad (1.5)$$

where V denotes the volume of 3-space and primes denote derivatives with respect to η . The classical equations obtained by minimizing the action (1.5) have a isotropic solution

$$a(\eta) = \left(\frac{\tilde{\rho}_r}{6} \right)^{1/2} \sqrt{16\pi G} \eta \quad , \quad \beta_{ij}(\eta) = 0 \quad , \quad (1.6)$$

of a radiation-dominated universe with radiation-energy density $\rho_r(\eta) = \tilde{\rho}_r / a^4(\eta)$. Since the function $F(\beta)$ is independent from a , the " φ -field" has no couplings with the "a-field". This is because of the invariance of the coupling between Φ and $g_{\mu\nu}$ under a conformal transformation, or more precisely, under the Weyl-rescaling,

$$\Phi \rightarrow \Omega^{-1}(x) \Phi \quad ,$$

$$g_{\mu\nu} \rightarrow \Omega^2(x) g_{\mu\nu} \quad .$$

As a result of this absence of a in $F[\beta]$, no φ -pairs are created in a isotropically expanding universe like (1.6) in agreement with Parker's argument [1]. In terms of the original scalar field Φ , the exact wave- function of a particle in such a isotropic universe is $1/a(\eta)$ times that of a free particle in a flat space-time.

Assuming small β , Hartle and Hu calculated the contribution of the one-loop graph of the φ -field, which is illustrated in the figure 1, to the gravitational effective action $S_{eff}[\alpha, \beta]$. This quantum correction term has a ultra-violet divergence,

$$- \frac{1}{960\pi^2(n-4)} \int d^4x \beta''_{ij} \beta'{}^i{}^j$$

when n -dimensional regularization method is used. The counter terms to subtract this divergence had to be either conformally invariant or pure divergence for $n = 4$. They showed that the right counter term is

$$S_c = \frac{\lambda \mu^{n-4}}{n-4} \int d^n x \sqrt{-g} (R_{\alpha\beta\gamma\delta} R^{\alpha\beta\gamma\delta} - R_{\alpha\beta} R^{\alpha\beta}) \quad , \quad (1.7)$$

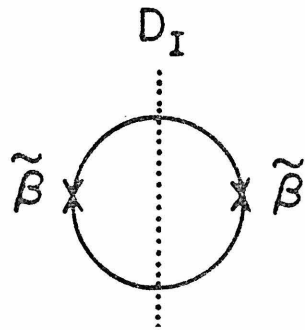


Figure 1: The one-loop graph treated by Hartle and Hu. The cut, which gives D_I , is shown by the dotted line.

where μ is an arbitrary constant of dimension $1/\text{length}$ and $\lambda=1/2880\pi^2$. The resulting finite action S_{eff} can be symbolically written as follows,

$$S_{eff}[\tilde{\alpha}, \tilde{\beta}, J] = S_0[\tilde{\alpha}] + \frac{1}{2} \tilde{\beta} D[\tilde{\alpha}] \tilde{\beta} + JGJ + JG\Gamma GJ\tilde{\beta} + \dots,$$

where

$S_0[\tilde{\alpha}]$: a real, nonlinear functional of $\tilde{\alpha}$,

$D[\tilde{\alpha}] = D_R[\tilde{\alpha}] + iD_I$: a complex operator,

G : the φ -propagator,

Γ : the $\beta\varphi\varphi$ proper vertex.

In the above, the source J for the φ -field is put in as was done in chapter II. Both S_0 and D have non-quadratic terms in $\tilde{\alpha}$ which come from the finite part of the counter term (1.7).

Using the effective action (1.8), the transition probability from the initial vacuum (II.2.1) to the final vacuum (II.2.2) is given by

$$\langle 0+ | 0- \rangle \equiv e^{iS_{eff}[\tilde{\alpha}, \tilde{\beta}, J] + i(\tilde{\alpha}A + \tilde{\beta}B)}, \quad (1.9)$$

where A is the source of $\tilde{\alpha}$ and B the source of $\tilde{\beta}$ *. The effective geometry $(\tilde{\alpha}, \tilde{\beta})$ is obtained from the equations,

$$\left. \frac{\delta S_{eff}}{\delta \tilde{\alpha}} \right|_{\tilde{\beta}, J} = -A, \quad (1.10)$$

$$\left. \frac{\delta S_{eff}}{\delta \tilde{\beta}} \right|_{\tilde{\alpha}, J} = -B, \quad (1.11)$$

* The signatures of sources differ from the convention in chapter II for technical reasons.

Substituting S_{eff} in the above by (1.8), we obtain a coupled nonlinear equations as follows;

$$\frac{\delta S_0(\tilde{\alpha})}{\delta \tilde{\alpha}} + \frac{1}{2} \tilde{\beta} \frac{\delta D(\tilde{\alpha})}{\delta \tilde{\alpha}} \tilde{\beta} = -A \quad , \quad (1.12a)$$

$$D(\tilde{\alpha})\tilde{\beta} = -B \quad , \quad (1.12b)$$

where we neglected the source J and higher order terms of $\tilde{\beta}$. In the small $\tilde{\beta}$ limit, the solutions $\tilde{\alpha}$ and $\tilde{\beta}$ can be written as a perturbation expansion about the zeroth order solutions $\tilde{\alpha}_0$ and $\tilde{\beta}_0$ as

$$\tilde{\alpha} = \tilde{\alpha}_0 + O(\tilde{\beta}_0^2), \quad (1.13a)$$

$$\tilde{\beta} = \tilde{\beta}_0 + O(\tilde{\beta}_0^2), \quad (1.13b)$$

where $\tilde{\alpha}_0$ is defined by

$$\frac{\delta S_0[\tilde{\alpha}_0]}{\delta \tilde{\alpha}_0} = -A, \quad (1.14a)$$

and $\tilde{\beta}_0$ by

$$D[\tilde{\alpha}_0]\tilde{\beta}_0 + O(J^2) = -B. \quad (1.14b)$$

At the lowest order of the perturbation expansion, α and β are decoupled: The function $\tilde{\alpha}_0$ is obtained from (1.14a) and $\tilde{\beta}_0$ is then given by (1.14b) where $\tilde{\alpha}_0$ is already known. At this order, $\tilde{\alpha}_0$ is real and $\tilde{\beta}_0$ is complex. Hartle and Hu [5,6] solved (1.14a) and (1.14b) numerically for $\tilde{\beta}_0 = \text{constant matrix} \times \text{scalar function of } \eta$. Then they discussed the total pair creation probability P , which is , in terms of $\tilde{\beta}_0$,

$$P = 1 - |\langle 0+ | 0- \rangle|^2 = 1 - e^{-R} \quad .$$

$$R = \frac{1}{2} \tilde{\beta}_0 D_I \beta_0 ,$$

which was derived by an argument similar to that used to derive the equation
(3.4) of chapter II.

2. Effective Geometry vs. Real Geometry

Hartle and Hu's model differs from the two-field model dealt in the previous chapter. Their model has three fields a , β , and φ , instead of two fields. The a -field couples to the β -field nonlinearly and the β -field couples to the φ -field. Thus, the β -field only is a source of pair creation, while both fields have configurations. These differences, however, are minor at the lowest order of the perturbation expansion (1.13a,b). In this section, we discuss the relation between the effective geometry and the real geometry along the lines of the argument given in the previous chapter.

First of all, equations (1.10) and (1.11) guarantee the following relations between the effective geometry ($\tilde{\alpha}$, $\tilde{\beta}$) and the corresponding field operators (\hat{a} , $\hat{\beta}$).

$$\tilde{\alpha} = \frac{\langle 0+ | \hat{a} | 0-\rangle}{\langle 0+ | 0-\rangle}, \quad (2.1a)$$

$$\tilde{\beta} = \frac{\langle 0+ | \hat{\beta} | 0-\rangle}{\langle 0+ | 0-\rangle}. \quad (2.1b)$$

as can be shown such as follows:

$$\begin{aligned} \langle 0+ | \hat{a} | 0-\rangle &= \left. \frac{\delta}{i\delta A} e^{i(S_{eff} + \tilde{\alpha}A + \tilde{\beta}B)} \right|_{B,J} \\ &= \left[\left. \frac{\delta \tilde{\alpha}}{i\delta A} \right|_{B,J} \left(\left. \frac{\delta S_{eff}}{\delta \tilde{\alpha}} \right|_{\tilde{\beta},J} + A \right) + \tilde{\alpha} + \left. \frac{\delta \tilde{\beta}}{i\delta A} \right|_{B,J} \left(\left. \frac{\delta S_{eff}}{\delta \tilde{\beta}} \right|_{\tilde{\alpha},J} + B \right) \right] e^{i(S_{eff} + \tilde{\alpha}A + \tilde{\beta}B)} \\ &= \tilde{\alpha} e^{i(S_{eff} + \tilde{\alpha}A + \tilde{\beta}B)} = \tilde{\alpha} \langle 0+ | 0-\rangle, \end{aligned}$$

As we did in section 4 of chapter II, we define the real configuration of the metric operators \hat{a} and $\hat{\beta}$, or the real configuration as the expectation values of \hat{a} and $\hat{\beta}$, in the initial vacuum state $|0-\rangle$:

$$\alpha^r \equiv \langle 0- | \hat{\alpha} | 0- \rangle , \quad (2.2a)$$

$$\beta^r \equiv \langle 0- | \hat{\beta} | 0- \rangle . \quad (2.2b)$$

These quantities are calculated by inserting the complete intermediate set of "+" states $\sum_j |j+\rangle \langle j+|$ as in (II.4.2).

In spite of the extra α -field, the argument in the previous chapter leading to the (II.4.4) applies to the above (2.2a,b) with minor modifications. The expression (II.3.7) for the one-pair creation amplitude is not changed at all, because the two-point propagator is now calculated as follows,

$$\begin{aligned} \langle 0+ | T(\varphi(1)\varphi(2)) | 0- \rangle &= \frac{\delta}{i\delta J(1)} \frac{\delta}{i\delta J(2)} e^{i(S_{eff} + \tilde{\alpha}A + \tilde{\beta}B)} \Big|_{A,B} \\ &= \frac{i\delta}{i\delta J(1)} \left[\left. \frac{\delta \tilde{\alpha}}{i\delta J(2)} \right|_{A,B} \left[\left. \frac{\delta S_{eff}}{\delta \tilde{\alpha}} \right|_{\tilde{\beta}, J} + A \right] + \left. \frac{\delta \tilde{\beta}}{i\delta J(2)} \right|_{A,B} \left[\left. \frac{\delta S_{eff}}{\delta \tilde{\beta}} \right|_{\tilde{\alpha}, J} + B \right] \right. \\ &\quad \left. + \left. \frac{\delta S_{eff}}{i\delta J(2)} \right|_{\tilde{\alpha}, \tilde{\beta}} \right] e^{i(S_{eff} + \tilde{\alpha}A + \tilde{\beta}B)} \Big|_{A,B} \\ &= \frac{i\delta}{i\delta J(1)} \left[\left. \frac{\delta S_{eff}}{i\delta J(2)} \right|_{\tilde{\alpha}, \tilde{\beta}} e^{i(S_{eff} + \tilde{\alpha}A + \tilde{\beta}B)} \right] \Big|_{A,B} \end{aligned}$$

where we denoted the independent variables which should be kept constant in the partial differentiation as $|_{A,B}$ etc. Equations (1.10) and (1.11) have also been used. From the effective action of (1.8), it is easy to see that only $\left. \frac{\delta S_{eff}}{\delta J(1)J(2)} \right|_{\tilde{\alpha}, \tilde{\beta}}$ survives for $J = 0$. Therefore, (II.3.7) holds. The projection operator at $\eta = +\infty$ of a particle with a momentum \mathbf{k} out of $\varphi(\eta_i x_i)$, is explicitly given by the following,

$$P_i = \lim_{\eta_i \rightarrow +\infty} \int d^3x \frac{ie^{-i(|\mathbf{k}_i| \eta_i - \mathbf{k}_i x_i)}}{\sqrt{2|\mathbf{k}_i|} (2\pi)^3} \left[\frac{\vec{\partial}}{\partial \eta_i} - \frac{\overleftarrow{\partial}}{\partial \eta_i} \right]. \quad (2.3)$$

Similarly, the operator F in (II.3.7) to obtain the creation amplitude of a pair of momentum (k_1, k_2) is

$$F_+ = - \frac{k_1^i k_1^j}{|k_1|} \delta^3(k_1+k_2) \int_{-\infty}^{+\infty} d\eta e^{i2|k_1|\eta}. \quad (2.4)$$

From (2.2b), we learn that

$$\beta^r = \tilde{\beta} - i \frac{\delta \tilde{\beta}}{\delta B} F^+ F^- \tilde{\beta}, \quad (2.5)$$

which corresponds to (II.4.5). In general, $\delta \tilde{\beta} / \delta B$ is a nonlinear function of \tilde{a} and $\tilde{\beta}$ because of the coupling seen in (1.12a,b). At the first order of the expansion (1.13a,b), however, (1.14b) leads to

$$\frac{\delta \tilde{\beta}}{\delta B} = \frac{\delta \tilde{\beta}_0}{\delta B} = - \frac{1}{D[a_0]}.$$

This is because \tilde{a}_0 satisfies (1.14a) and therefore is independent from B . In terms of \tilde{a}_0 and $\tilde{\beta}_0$, (2.5) is reduced to

$$\beta^r = \tilde{\beta}_0 + \frac{i}{D[\tilde{a}_0]} F^+ F^- \tilde{\beta}_0 + O(\tilde{\beta}_0^2). \quad (2.6)$$

The only difference between (2.6) and (II.4.5) is that the propagator i/D is now explicitly time-dependent because of \tilde{a}_0 . Therefore, the energy conservation rule (II.3.15) does not necessary hold. However, under the assumption that the a -field itself does not create any β -quanta, $i/D[\tilde{a}_0]$ does not connect the negative frequency part to the positive frequency part, and thus (II.3.15) holds. It should be noted that in deriving (2.6), we virtually used such an assumption: If this assumption is not satisfied, we have to take into account the contribution of the graph with intermediate β -quanta such as the one illustrated in figure 2.

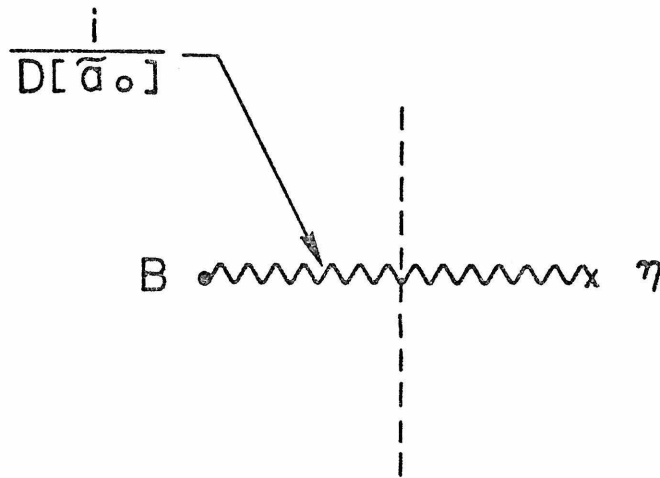


Figure 2: An extra contribution to (2.6) when the a -field can be a source of β -quanta.

Under this assumption, results (II.4.6a,b) and (II.4.7) hold in our model. Especially, (II.4.7) gives the equation for β^r . The imaginary part of $D[\tilde{\alpha}_0]$ comes from finite part of the graph in figure 1, which is proportional to

$$\int_0^1 dx \ln(-i\varepsilon - p^2 x(1-x)) \sim \ln(-3i\varepsilon - p^2) + \text{constants} ,$$

where p is the four-momentum into the vertex $\tilde{\beta}^2$. Since we assume spatial homogeneity, the space portion of p is zero. The exact $D[\tilde{\alpha}_0]_{\eta,\eta'}$ in equation (1.14b) is as follows,

$$D[\tilde{\alpha}_0]_{\eta,\eta'} = D_0[\tilde{\alpha}_0]_{\eta,\eta'} - \frac{3\lambda}{\pi} \left[\frac{\partial}{\partial \eta} \right]^2 F(\eta-\eta') \left[\frac{\partial}{\partial \eta'} \right]^2 , \quad (2.7)$$

with

$$F(\eta-\eta') = \int_C dp^0 e^{-ip^0(\eta-\eta')} \ln \frac{-3i\varepsilon - p^0{}^2}{\mu^2} . \quad (2.8)$$

The operator D_0 is nonlinear in $\tilde{\alpha}_0$, local, and real. The scale μ comes from the contour term (1.7) to give the dimensionless argument of the logarithm. The contour C is the same as the one given in the figure II.2 except that now $m=0$ as is seen by inspecting the action in (1.1) or (1.3). $F(\eta-\eta')$ is explicitly calculable with the help of an appropriate regularization scheme. For example [8],

$$\begin{aligned} F(\eta) &= 2 \int_0^\infty d\omega \cos\omega\eta \ln \frac{\omega}{\mu} - i\pi \int_{-\infty}^\infty d\omega e^{-i\omega\eta} \\ &\equiv \lim_{\alpha \rightarrow 0} 2 \int_0^\infty d\omega \cos\omega\eta e^{-\alpha\omega} \ln \frac{\omega}{\mu} - 2i\pi^2 \delta(\eta) \\ &\equiv \lim_{\alpha \rightarrow 0} \left[-\frac{2}{\eta^2 + \alpha^2} \left(\alpha\eta + \frac{\alpha}{2} \ln(\eta^2 + \alpha^2) + \eta \tan^{-1} \frac{\eta}{\alpha} \right) \right] - 2i\pi^2 \delta(\eta) \\ &= -\pi P \frac{1}{|\eta|} - 2i\pi^2 \delta(\eta) . \end{aligned}$$

where $\gamma=0.5772156649\dots$ is the Euler's constant. The above expression can also be obtained by deforming the contour under the same regularization condition. For $\eta < 0$, for instance, the contour c is deformed to C' in the figure (II.2), which picks up the discontinuity of the integrand:

$$F(\eta) = -2i\pi \int_{-\infty}^0 d\omega e^{-i\omega\eta} = -2i\pi \left[P \frac{i}{\eta} + \pi\delta(\eta) \right]. \quad (2.10)$$

The integro-differential operator D^r in (II.4.7) has the same contour C^r with $1/D^r$. Thus, D^r is written in a manner similar to (2.7),

$$D^r[\tilde{a}_0]_{\eta\eta'} = D_0[\tilde{a}_0]_{\eta\eta'} - \frac{3\lambda}{\pi} \left[\frac{\partial}{\partial\eta} \right]^2 F^r(\eta-\eta') \left[\frac{\partial}{\partial\eta'} \right]^2, \quad (2.8)$$

$$F^r(\eta-\eta') = \int_{C^r} dp^0 e^{-ip^0(\eta-\eta')} \ln \frac{-3i\varepsilon - p^{02}}{\mu^2}.$$

For the purpose of illustration, we calculate F^r by two methods that correspond to (2.9) and (2.10). First, the direct calculation shows the following,

$$F^r(\eta) = 2 \int_0^\infty d\omega \cos\omega\eta \ln \frac{\omega}{\mu} - i\pi \int_{-\infty}^\infty d\omega \varepsilon(\omega) e^{-i\omega\eta}$$

$$= -\pi P \frac{1}{|\eta|} - i\pi \left[-iP \frac{1}{\eta} \right] = -2\pi\vartheta(\eta) P \frac{1}{\eta}, \quad (2.11)$$

where $\varepsilon(\omega) \equiv \omega/|\omega|$. By the method of contour deformation, we learn that

$$F^r(\eta) = \vartheta(\eta) \left[-2i\pi \int_{-\infty}^\infty d\omega \varepsilon(\omega) e^{-i\omega\eta} \right] = -2\pi\vartheta(\eta) P \frac{1}{\eta}, \quad (2.12)$$

which agrees with (2.11).

For a^r of (2.2a), the same method gives a result analogous to (2.5),

$$a^r = \tilde{a} - i \frac{\delta\tilde{\beta}}{\delta A} F^+ F^- \tilde{\beta}. \quad (2.13)$$

Using the expansion (1.13), we obtain

$$\tilde{a} = \tilde{a}_0 + O(\tilde{\beta}_0^2) - i \frac{\delta \tilde{\beta}_0}{\delta A} F^+ F^- \tilde{\beta}_0 + \text{higher orders}$$

Since, from (1.14b),

$$\frac{\delta \tilde{\beta}_0}{\delta A} = - \left[\frac{\delta}{\delta A} \frac{1}{D[\tilde{a}_0]} \right] B = - \frac{\delta \ln D[\tilde{a}_0]}{\delta A} \tilde{\beta}_0 \quad ,$$

we learn that

$$a^r = \tilde{a}_0 + O(\tilde{\beta}_0^2) \quad . \quad (2.14)$$

The above a^r is real up to first order in $\tilde{\beta}_0$, since \tilde{a}_0 is real.

In summary, the real geometry (a^r, β^r) was related to the effective geometry $(\tilde{a}, \tilde{\beta})$ up to first order of the perturbation expansion (1.13a,b). The assumption that the configuration \tilde{a}_0 does not create any β -quanta has been used. For the higher orders of $\tilde{\beta}_0$, not only the numerical calculation of $\tilde{\beta}$ becomes very complicated, but also $\tilde{\beta}^3$ term of S_{eff} becomes important. Nevertheless, all the expected features of the model are already exhibited at the current order of the perturbation expansion. Therefore, even though the relation between the effective geometry and the real geometry could be extended to higher orders, I believe that higher orders are not of practical interest.

References for chapter III

- [1] L. Parker, Phys. Rev. 164 (1969) 1057.
- [2] Ya. B. Zel'dovich, Pis'ma Zh. Eksp. Theor. Fiz. 12 (1970) 443 [JETP Lett. 12 (1970) 307]; Ya. B. Zel'dovich and A. A. Starovinsky, Zh. Eksp. Theor. Fiz. 61 (1971) 2161 [Sov. Phys. - JETP 34 (1971) 1159], Pis'ma. Zh. Eksp. Theor. Fiz. 26 (1977) 373 [JETP Lett. 26 (1977) 251]; B. L. Hu and L. Parker, Phys. Rev. D17 (1978) 933.
- [3] M. V. Fischetti, J. B. Hartle and R. L. Hu, Phys. Rev. D20 (1979) 1757.
- [4] J. B. Hartle and B. L. Hu, Phys. Rev. D20 (1979) 1772.
- [5] J. B. Hartle and B. L. Hu, Phys. Rev. D21 (1980) 2756.
- [6] J. B. Hartle, Phys. Rev. D22 (1980) 2091.
- [7] J. B. Hartle, UCSB preprint, UCSB TH-50 (1980).
- [8] "Table of Integral Transforms" (Bateman Manuscript Project) vol.1, page 18 (McGraw-Hill, 1954).

IV. Vacuum Bubble Expansion

1 Introduction

In certain models of elementary particles, there exist degenerate or metastable vacua. They are vacua in the sense that any one of them is not obtained by adding infinitesimal excitations, or a finite number of particles, to any other state in the model. However, they are connected by finite excitations, or displacement of fields. In analogy with the WKB-method for tunneling amplitudes in quantum mechanics, the transition amplitudes between the different vacua are given by examining the finite displacements that connect the vacua. The steady states of the model, which are called the true vacua, depend on the properties of the transition amplitudes.

In pure gauge field theories, we have degenerate discrete vacua that have different topological properties. In the $SU(3)$ Yang-Mills theory of the strong interaction, for example, there are infinite number of vacua $|n\rangle$, where n is an integer varying from $-\infty$ to $+\infty$. The m -instanton solution [1], which is an Euclidean solution with a finite action $S_E(m)$ and a topological number m , connects an initial vacuum $|n, -\rangle$ and a final vacuum $|n+m, +\rangle$,

$$\langle n+m, + | n, - \rangle = T_m \propto e^{-S_E(m)} . \quad (1.1)$$

Since the transition amplitudes depend only on the difference of the indices of the vacuum, a true vacuum $|\mathcal{V}\rangle$ is a superposition of the discrete of vacua given as follows,

$$|\vartheta\rangle = N \sum_{n=-\infty}^{\infty} e^{in\vartheta} |n\rangle ,$$

where $0 \leq \vartheta < 2\pi$ and N is the normalization factor. In fact,

$$\begin{aligned} \langle \vartheta', + | \vartheta, - \rangle &= |N|^2 \sum_{n, n'} e^{i(n\vartheta - n'\vartheta')} \langle n' + | n, - \rangle \\ &= |N|^2 \sum_{n, n'} T_{n-n'} e^{i\frac{1}{2}[(n-n')(\vartheta+\vartheta') + (n+n')(\vartheta-\vartheta')]} \\ &\propto \delta(\vartheta - \vartheta') . \end{aligned}$$

Similar mechanisms have been proposed for models with Higgs mechanism [2]. In models that have monopole solutions of finite action [3] in Euclidean space-time, the different degenerate vacua also have a transition amplitude like (4.1). Thus, it was suggested that the true vacua may be a mixture of the usual vacua that have definite expectation values of Higgs fields.

When a model has non-degenerate vacua, there is no mixing, and the true vacuum is the state with the lowest energy density. A vacuum state of higher energy density, which is called the false vacuum [3], decays in time. This decay is realized by nucleation, creation of bubbles of the true vacuum in the false vacuum surroundings. A famous analogy is the boiling of superheated fluids [4]. This nucleation mechanism for phase transition in quantum field theory was first suggested by Volosin et. al. [5]. Coleman and Callan [6,7] developed a method to calculate the decay rate of false vacuum. In contrast to (1.1), they discussed the amplitude,

$$\langle \text{false vacuum}, T | \text{false vacuum}, 0 \rangle \propto e^{-iE_f T} .$$

The quantum correction to E_f was shown to have an imaginary part in the Euclidean path-integral formalism. The false vacuum decay rate Γ per unit time

is obtained from E_f as,

$$\Gamma = -2\text{Im}E_f.$$

Coleman [6] argued on basis of a classical analysis that once a bubble is created, all the energy released in converting the false vacuum to the true vacuum is used to accelerate the wall, and that no "roiling sea of mesons" is left behind it. The generalization to finite temperature were discussed by Linde [8].

This phase transition from the false vacuum to the true vacuum plays an important role in cosmology. Most of the models with spontaneous symmetry breaking at $T = 0$ have their original symmetry restored at high temperature [9]. Thus, the early universe is in the symmetric phase of the theory. As the universe cools down to a temperature of the grand-unified scale $\sim 10^{15}$ GeV, the symmetry-broken phases become the true vacua. If the nucleation rate is high, many bubbles with different VEVs are created at the same time. As each bubble expands and collides with each other, "knots" of different VEVs, monopoles [10], are created between them. The number of monopoles is of the same order as that of the bubbles and therefore in conflict with observations [11]. An alternative scenario, the inflationary universe, has been proposed by Guth and others [12]. Their idea was to have a small nucleation rate so that the universe is dominated by a few large bubbles. The monopole problem is thus solved. Furthermore, due to the high energy density of the false vacuum, the early universe undergoes an exponential expansion state for a relatively long time. Therefore, the horizon and flatness problems seem to be avoided. A difficulty of this scenario is that if Coleman's conclusion of no "roiling sea of mesons" is to be believed, then the energy of false vacua should be released only when the walls of the few large bubbles collide. This leads to a large scale inhomogeneity and anisotropy [13]. To avoid this difficulty, several other scenarios has been

proposed [14, 15].

It should be noted that Coleman's argument on the real-time behavior of a bubble is a classical one. Particle production is quantum phenomenon. Thus, it is natural that Coleman did not find the roiling sea of mesons. Since Coleman's conclusion is one of the bases of constructing models of the early universe and the elementary particles, it is important to take quantum effects into account and to see whether the energy obtained by the conversion is still concentrated on the wall or not. The purpose of this chapter is to describe an attempt to evaluate quantum effects, especially pair creation.

In the next section, we briefly describe Coleman's work [6] on the real-time behavior of the wall in connection with the earlier works by Volosin and others [5]. The method for calculating the nucleation rate [7] is also outlined for completeness. In Section 3, we apply the effective action method developed in chapter II to this problem. Three field equations are given corresponding to different physical situations. Section 4 gives a semi-classical treatment of the bubble expansions. Also the asymptotic behavior of the bubble and pair creation rates is examined under some assumptions. Finally in section 5 we discuss on results.

2. Quantum Creation and Classical Expansion of a Vacuum Bubble

The simplest model that has all the essential features for the decay of the false vacua is that of a single scalar field φ with the following action at a tree level [16, 5, 6],

$$S = \int d^4x \left\{ \frac{1}{2} (\partial_\mu \varphi)^2 - V(\varphi) \right\}. \quad (2.1)$$

The potential $V(\varphi)$ has two minima φ_+ and φ_- , the former having an energy density ε higher than the latter, as is illustrated in Fig. 1.

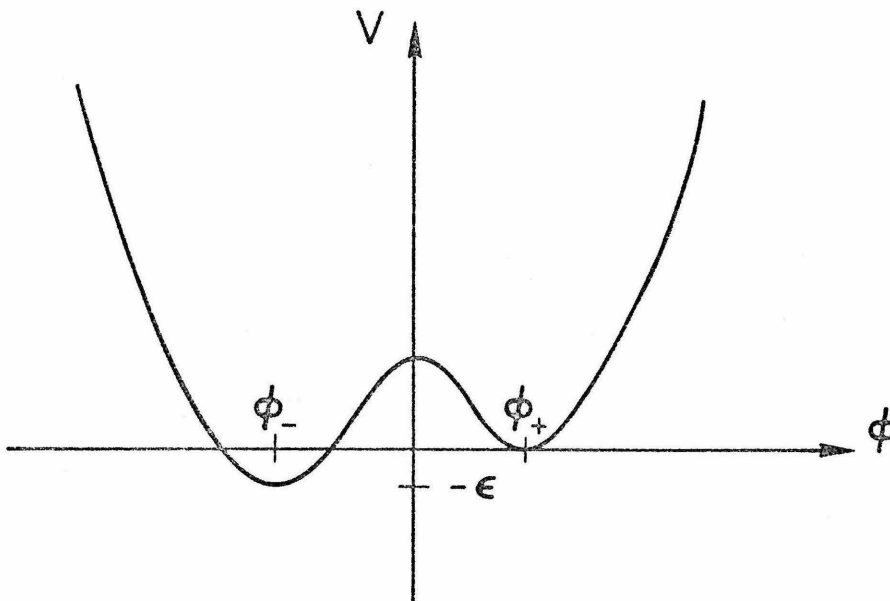


Figure 1: A potential $V(\varphi)$ that has a stable vacuum φ_- and a meta-stable vacuum φ_+ .

The following $V(\varphi)$ is commonly used,

$$V(\varphi) = \frac{\lambda}{8}(\varphi^2 - a^2)^2 + \frac{\varepsilon_0}{2a}(\varphi - a), \quad (2.2)$$

which will be explained later ((4.3)).

Consider a bubble of true vacuum $\langle\varphi\rangle = \varphi_-$ surrounded by false vacuum $\langle\varphi\rangle = \varphi_+$ with a thin wall, a transition region that is narrow relative to the radius of the bubble, separating the two vacua. The energy E^b of such a bubble relative to the homogeneous, i.e., complete false vacuum, is given by the following [5],

$$E^b = \frac{4\pi S_1 R^2}{\sqrt{1-\dot{R}^2}} - \frac{4\pi\varepsilon}{3} R^3, \quad (2.3)$$

where $R(t)$ is the radius of the bubble in the c.m. frame and $\dot{R} \equiv dR/dt$. The first term includes the surface-tension and the Lorentz factor due to the motion of the wall. S_1 is the rest energy of the bubble wall per unit area. The second term is the energy gain due to the difference in the energy density between the true and the false vacua. By conservation of energy, $E^b=0$, then the solution to (2.2) is

$$R = \sqrt{R_0^2 + (t-t_0)^2}, \quad (2.4)$$

where R_0 is the radius of the bubble at rest ($t = t_0$),

$$R_0 = \frac{3S_1}{\varepsilon}. \quad (2.5)$$

Therefore, once a bubble is created, regardless of whether it is shrinking ($t < t_0$), at rest ($t = t_0$) or expanding ($t > t_0$) at the time of the creation, it blows up as $t \rightarrow \infty$ (see the figure 2). This is because all the energy released from the false vacuum is used to accelerate the wall. The wall is accelerated outward

because the wider region of the true vacuum is energetically favored. From (2.5) we also note that the thin wall approximation is satisfied by the small ε compared to the height and width of the potential barrier between ϕ_- and ϕ_+ . This is because as $\varepsilon \rightarrow 0$, the thickness of the wall and S_1 are governed by the shape of the potential barrier and therefore finite, while the minimum radius R_0 diverges.

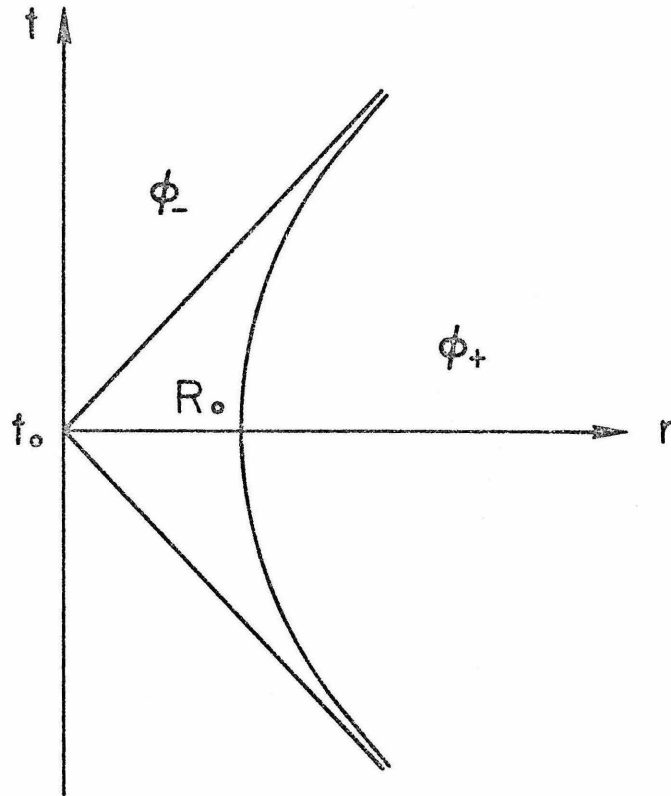


Figure 2: The "world line" of the bubble wall (2.4).

The prescription for the nucleation rate was given by Callan and Coleman [7]. In Euclidean space-time, there is a localized hyperspherical solution φ_1 which has the following property [6, 17],

$$\varphi_1(\tau, t) \begin{cases} \sim \varphi_- & \text{for } \rho \equiv \sqrt{\tau^2 + r^2} \sim 0 \\ \rightarrow \varphi_+ & \text{as } \rho \rightarrow \infty \end{cases} \quad (2.6)$$

where $\tau = -it$ is the Euclidean time. The energy E_f of the false vacuum state gets a quantum correction due to the presence of bubbles. They can be calculated as follows,

$$\begin{aligned} \langle \varphi_+, \tau_f | \varphi_+, \tau_i \rangle &\sim e^{-E_f(\tau_f - \tau_i)} \\ &\propto \int [d\varphi] e^{-S_E[\varphi]} \end{aligned}$$

where $S_E[\varphi]$ is the Euclidean action and the functional integral over φ has the boundary condition $\varphi(\tau = \tau_i, \tau_f) = \varphi_+$. Let $\tilde{\varphi} = \varphi - \varphi_1$ be perturbations about the 1 bubble solution (2.6), then naive integration over $\tilde{\varphi}$ gives

$$\int [d\tilde{\varphi}] e^{-S_E[\varphi_1] - \tilde{\varphi}(-\partial^2 + V''(\varphi_1))\tilde{\varphi}} \propto e^{-S_E[\varphi_1]} (\det(-\partial^2 + V''(\varphi_1)))^{-1/2}. \quad (2.7)$$

The determinant is a product of all the eigenvalues of the operator $-\partial^2 + V''(\varphi_1)$. There are zero eigenmodes which correspond to displacements of the original solution,

$$\tilde{\varphi}_0 = \frac{d\varphi_1}{dx} \delta x. \quad (2.8)$$

Displacements are actually treated by considering the coordinates of the center of the solution φ_1 as a collective coordinate in the functional integral in (2.7) [18]. Therefore, zero eigenmodes do not appear in the r.h.s. of (2.7). The modes (1.6) have nodes, and therefore are not lowest eigenmodes: There exist negative

eigenvalues, which make (2.7) complex. The Gaussian integration of the l.h.s. of (2.7) actually diverges for these negative eigenvalues. A convergent expression is obtained by modifying the integration "contour" in complex φ -functional space. After summing the contributions of other multicentered solutions, Callan and Coleman obtained

$$\text{Im}E_f = - \frac{VS_E[\varphi_1]^2}{8\pi^2} e^{-S_E[\varphi_1]} \left| \frac{\det'(-\partial^2 + V''(\varphi_1))}{\det(-\partial^2 + V''(\varphi_+))} \right|^{-1/2},$$

where V is the volume of the space and \det' denotes that the zero eigenvalues are excluded.

The solution (2.6) in Euclidean space-time is related to the bubble in real time (2.4) by analytic continuation. In real time, φ_1 is a function of $\rho = \sqrt{-t^2 + r^2}$. Thus, the surfaces of constant φ_1 are hyperboloids like the one illustrated in Fig. 2. In fact, if we assume that the solution (2.6) has a narrow transition region at around $\rho \sim R$, φ_1 is obtained so as to minimize the Euclidean action S_E , which is given as follows,

$$S_E = 2\pi^2 \int_0^\infty \rho^3 d\rho \left[\frac{1}{2} \left(\frac{d\varphi_1}{d\rho} \right)^2 + V \right] = \pi^2 R^3 S_1 - \frac{\pi^2}{2} R^4 \varepsilon. \quad (2.9)$$

In the above, we used

$$\left(\frac{d\varphi_1}{d\rho} \right)^2 \sim S_1 \delta(\rho - R),$$

and

$$U(\rho) \sim -\varepsilon \mathcal{V}(R - \rho). \quad (2.10)$$

The constants S_1 and ε in (2.10) are the same as the ones in (2.3) because the energy E of a bubble at rest is given by

$$E = 4\pi \int_0^\infty r dr \left[\frac{1}{2} \left(\frac{d\varphi_1}{dr} \right)^2 + V \right] = 4\pi S_1 R^2 - \frac{4\pi}{3} R^3.$$

The action (2.9) is minimized by $R = 3S_1/\varepsilon$, thus the wall is located at

$$\rho = \sqrt{-t^2 + r^2} = \frac{3S_1}{\varepsilon},$$

in agreement with (2.4,5).

3. Quantum Correction to the Bubble Equation of Motion

As was explained in the previous section, the bubble solution in real-time, $\varphi_1(\rho = \sqrt{-t^2 + r^2})$, is a solution that minimizes the classical action (1.2). Therefore, φ_1 satisfies the following equation,

$$\partial_\mu \partial^\mu \varphi_1 + \frac{\partial V(\varphi_1)}{\partial \varphi_1} = 0. \quad (3.1)$$

Since no quantum correction is considered, this φ_1 in the above equation is related to the quantum field operator $\hat{\varphi}$ as

$$\varphi_1 = \frac{\langle 0+ | \hat{\varphi} | 0-\rangle}{\langle 0+ | 0-\rangle} = \langle 0- | \hat{\varphi} | 0-\rangle$$

in the limit $\hbar \rightarrow 0$. This section discusses the $O(\hbar^1)$ correction to the above matrix element.

In our simple model (1.2), there is only one field φ in contrast to the two-field model discussed in chapter II. The fluctuation φ^f of the φ -field on the background $\tilde{\varphi}$ corresponds to the φ -field in the two-field model,

$$\varphi^f = \varphi - \tilde{\varphi}. \quad (3.2)$$

In spite of this difference of models, most of the results obtained in chapter II apply to our model at the order of the first quantum correction. The effective action $S_{eff}[\tilde{\varphi}]$ is defined as follows

$$e^{\frac{i}{\hbar}(S_{eff}[\tilde{\varphi}] - \tilde{\varphi}J)} \equiv \langle 0+ | 0-\rangle_J = \int [d\varphi] e^{\frac{i}{\hbar}(S[\varphi] - \varphi J)}, \quad (3.3)$$

where $\tilde{\varphi}$ is defined by

$$\frac{\delta S_{eff}[\tilde{\varphi}]}{\delta \tilde{\varphi}} = J. \quad (3.4)$$

In (3.3), an appropriate normalization is assumed and \hbar is inserted for convenience. Definition (3.3) can be modified to yield a compact expression for $S_{eff}[\tilde{\varphi}]$,

$$S_{eff}[\tilde{\varphi}] = -i \hbar \ln \left[\int [d\varphi] e^{\frac{i}{\hbar}(S[\varphi] - (\varphi - \tilde{\varphi})J)} \right]. \quad (3.5)$$

We expand $S[\varphi]$ in terms of the fluctuation φ^f of (3.2),

$$S[\varphi] = S[\tilde{\varphi}] + \frac{\delta S[\tilde{\varphi}]}{\delta \tilde{\varphi}} \varphi^f + \frac{1}{2} \varphi^f D[\tilde{\varphi}] \varphi^f + S_{int}[\tilde{\varphi}, \varphi^f], \quad (3.6)$$

where $S_{int}[\tilde{\varphi}, \varphi^f]$ contains terms with cubic or higher powers in φ^f . After substituting (3.6) into (3.5), we obtain

$$S_{eff}[\tilde{\varphi}] = S[\tilde{\varphi}] - i \hbar \ln \left[\int [d\varphi^f] \exp \frac{i}{\hbar} \left[\frac{1}{2} \varphi^f D[\tilde{\varphi}] \varphi^f + S_{int}[\tilde{\varphi}, \varphi^f] + \left(\frac{\delta S[\tilde{\varphi}]}{\delta \tilde{\varphi}} - J \right) \varphi^f \right] \right].$$

Thus, the quantum correction $S^f[\tilde{\varphi}] \equiv S_{eff}[\tilde{\varphi}] - S[\tilde{\varphi}]$ satisfies the following self-consistent equation [19].

$$S^f[\tilde{\varphi}] = -i \hbar \ln \left[\int [d\varphi^f] \exp \frac{i}{\hbar} \left[\frac{1}{2} \varphi^f D[\tilde{\varphi}] \varphi^f + S_{int}[\tilde{\varphi}, \varphi^f] - \frac{\delta S^f[\tilde{\varphi}]}{\delta \tilde{\varphi}} \varphi^f \right] \right]. \quad (3.7)$$

The \hbar -expansion for $S^f[\tilde{\varphi}]$ is obtained by starting from the zeroth order solution, $S^f[\tilde{\varphi}] = 0$, and iterating (3.7). The first order solution is

$$S^f[\tilde{\varphi}] = -i \hbar \ln \left[\int [d\varphi^f] \exp \frac{i}{\hbar} \left[\frac{1}{2} \varphi^f D[\tilde{\varphi}] \varphi^f + S_{int}[\tilde{\varphi}, \varphi^f] \right] \right].$$

This expression contains still higher power of \hbar . The expansion in \hbar is equivalent to the expansion in the number of loops [20]. The lowest term is the one-loop term, which yields

$$S^f[\tilde{\varphi}] = i \hbar \ln \sqrt{\det D[\tilde{\varphi}]} + C,$$

$$= \frac{i\hbar}{2} \text{Tr} \ln D[\tilde{\varphi}] + C,$$

where C is constant.

The effective configuration $\tilde{\varphi}$ corrected to first order in \hbar is obtained by minimizing the effective action,

$$S_{eff}[\tilde{\varphi}] = S[\tilde{\varphi}] + \frac{i\hbar}{2} \text{Tr} \ln D[\tilde{\varphi}] + C. \quad (3.8)$$

However, since $\tilde{\varphi}$ is space-time dependent, we usually can not evaluate $\text{Tr} \ln$ term exactly. If that is the case, we have to expand and take a few terms of the $\text{Tr} \ln$ term. Since only a few terms can be taken into account, the expansion has to be such that the physical picture is right: From the action (1.2), we learn that

$$D[\tilde{\varphi}] = -\partial_\mu \partial^\mu - \frac{\partial^2 V(\tilde{\varphi})}{\partial \tilde{\varphi}^2}.$$

Consider the following expansion of the $\text{Tr} \ln$ term of (3.8),

$$\begin{aligned} \text{Tr} \ln D[\tilde{\varphi}] &= \text{Tr} \ln(-\partial_\mu \partial^\mu - m^2) + \text{Tr} \ln \left[1 - \frac{1}{-\partial_\mu \partial^\mu - m^2} \left(\frac{\partial^2 V(\tilde{\varphi})}{\partial \tilde{\varphi}^2} - m^2 \right) \right] \\ &= C' + \sum_{n=1}^{\infty} \frac{1}{n} \text{Tr} \left[\frac{1}{-\partial_\mu \partial^\mu - m^2} \left(\frac{\partial^2 V(\tilde{\varphi})}{\partial \tilde{\varphi}^2} - m^2 \right) \right]^n, \end{aligned} \quad (3.9)$$

where C' and m^2 are constants. The series in (3.9) is graphically represented in Fig. 3. The first term vanishes in dimensional regularization. The second term has a cut C . Since we will use a few terms of the expansion (3.9), this cut has to correspond to the contribution of the physical intermediate states. This is also important for the discussion of the real configuration φ^r . Therefore, m has to be chosen as a mass for created particles. However, there are two masses in this theory, the mass m_+ of the excitations in the false vacuum and the mass

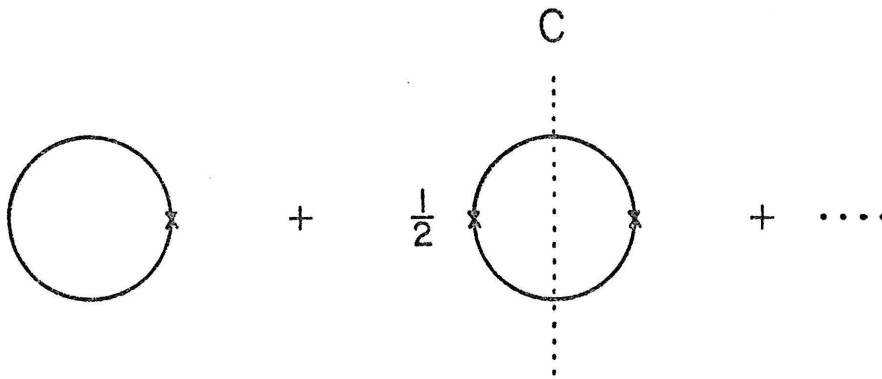


Figure 3: The series of (3.9). The solid lines represent $\frac{1}{-\partial^\mu \partial_\mu - m^2}$ and the vertex

$$\frac{\partial^2 V(\varphi)}{\partial \tilde{\varphi}^2} - m^2.$$

vacuum and the mass m_- of the excitations in the true vacuum. The choice has to be self-consistent: If we choose m to be m^+ , the result has to be such that both particles of the created pairs mainly go out of the bubble. And if m_- , both have to go into or remain inside the bubble.

In both cases, the effective action is approximated as the following,

$$S_{eff}[\tilde{\varphi}] = S[\tilde{\varphi}] + \frac{1}{2} \left[\frac{\partial^2 V(\tilde{\varphi})}{\partial \tilde{\varphi}^2} - m_{\pm}^2 \right] K_{\pm} \left[\frac{\partial^2 V(\tilde{\varphi})}{\partial \tilde{\varphi}^2} - m_{\pm}^2 \right], \quad (3.10)$$

where the kernel K_{\pm} is

$$\begin{aligned} K_{\pm} &\equiv \frac{i}{2} \left[\frac{1}{-\partial^{\mu}\partial_{\mu} - m_{\pm}^2} \right]^2 \quad (\text{symbolically}), \\ &= \int \frac{d^4 k}{(2\pi)^4} e^{-ik(x-y)} K_{\pm}(k^2) \quad (\text{in coordinate space}). \end{aligned}$$

Using dimensional regularization with $n = 4 + 2\omega$, $K(k^2)$ is given by

$$\begin{aligned} K(k^2) &= \frac{i}{2} \int \frac{d^n q}{(2\pi)^n} \frac{1}{q^2 - m_{\pm}^2 + i\varepsilon} \frac{1}{(q+k)^2 - m_{\pm}^2 + i\varepsilon} \\ &= \frac{-1}{32\pi^2} \left[\frac{1}{4\pi} \right]^{\omega} \Gamma(-\omega) - \frac{1}{32\pi^2} \int_0^1 dx \ln(m_{\pm}^2 + i\varepsilon - k^2 x(1-x)). \end{aligned} \quad (3.11)$$

The above $K(k^2)$ has an imaginary part,

$$\text{Im}K_{\pm}(k^2) = \frac{1}{32\pi} \vartheta(k^2 - 4m_{\pm}^2) \sqrt{1 - \frac{4m_{\pm}^2}{k^2}}. \quad (3.12)$$

Since the highest power of $\tilde{\varphi}$ in V is 4 as required by renormalizability, the second term of the r.h.s. of (3.10) is also $\tilde{\varphi}^4$ at most. Thus, the divergence of $O(1/\omega)$ in (3.11) can be absorbed into the parameters in $S[\tilde{\varphi}]$. The equation for the effective field configuration $\tilde{\varphi}$ is obtained by minimizing (3.10).

$$-\partial_\mu \partial^\mu \tilde{\varphi} + \frac{\partial V(\tilde{\varphi})}{\partial \tilde{\varphi}} + \frac{\partial^3 V(\tilde{\varphi})}{\partial \tilde{\varphi}^3} K_\pm \left[\frac{\partial^2 V(\tilde{\varphi})}{\partial \tilde{\varphi}^2} - m_\pm^2 \right] = 0. \quad (3.13)$$

Since K_\pm is complex, $\tilde{\varphi}$ is complex as is expected. Since the graph treated here is the same as the one used in the analysis in chapter II, the equation for the real configuration φ^r is obtained from (3.12) by replacing K_\pm by a retarded real kernel K_\pm^r .

$$K_\pm^r = \text{constant} - \frac{1}{32\pi} \int_0^1 dx \ln(m_\pm^2 - i\varepsilon k_0 - k^2 x(1-x)). \quad (3.14)$$

There is another possible situation in which one particle of the pair goes inside the bubble and the other outside. In this case, neither of the choices m_+ or m_- is appropriate. There is a prescription to treat the two vacua symmetrically, which was originally found by the author [21] for the pair creation problem by strong electric fields, i.e., the Klein problem. The idea is to rearrange the perturbation series such that both Green's functions, one with mass m_+ and one with m_- , appear in the same graph. That goes as follows: First, we start from the perturbation series (3.9) with m being one of the masses, say, m_+ . The vertex κ can be divided into two parts,

$$\begin{aligned} \kappa &= \frac{\partial^2 V(\tilde{\varphi})}{\partial \tilde{\varphi}^2} - m_+^2 \\ &= (m_-^2 - m_+^2) + \left[\frac{\partial^2 V(\tilde{\varphi})}{\partial \tilde{\varphi}^2} - m_-^2 \right] \\ &\equiv \square + \circ \end{aligned}$$

We decompose each term in the expansion (3.9) according to the following procedure:

- (i) Pick up a vertex as a starting point to go around the circle clockwise. The coefficient $1/n$ is canceled by the n -possible choices.
- (ii) The next vertex \times is decomposed into \square and \circ . Thus, two graphs are generated.
- (iii) In each of the graphs generated at the step (ii), if the second vertex is \square , the third vertex \times is decomposed into two.
- \vdots
- (n) In each of the graphs generated at the step $(n-1)$, if the $(n-1)$ th vertex is either \times or \square , the n th vertex is decomposed into two.

The steps (i) ~ (iii) is illustrated in Fig. 4. The result of this decomposition for the first four terms of the expansion in (3.9) is given in Fig. 5. Because of the step (n), for each graph of definite \times 's and \circ 's, we have an infinite series of graphs due to all possible numbers of \square lined up after the \times 's. Each such series of graphs can be summed up by using the Green's function for a particle with mass m_{\pm} ,

$$\sum_{l=0}^{\infty} \left[\frac{1}{-\partial_{\mu}\partial^{\mu}-m_{\pm}^2} (m_{\pm}^2 - m_{\mp}^2) \right]^l \frac{1}{-\partial_{\mu}\partial^{\mu}-m_{\pm}^2} = \frac{1}{-\partial_{\mu}\partial^{\mu}-m_{\pm}^2} \quad (3.15)$$

Figure 6 gives the graphical representation of the above. The first four terms of the resulting rearranged series are given in Fig. 7. This series has the following physical interpretation: Since the mass of the fluctuation is given by the curvature of the potential,

$$m_{\pm}^2 = \left. \frac{\partial^2 V(\tilde{\varphi})}{\partial \tilde{\varphi}^2} \right|_{\tilde{\varphi} = \varphi_{\pm}}$$

Then the vertex \times is zero in the space-time region where $\tilde{\varphi} = \varphi_{+}$, and the

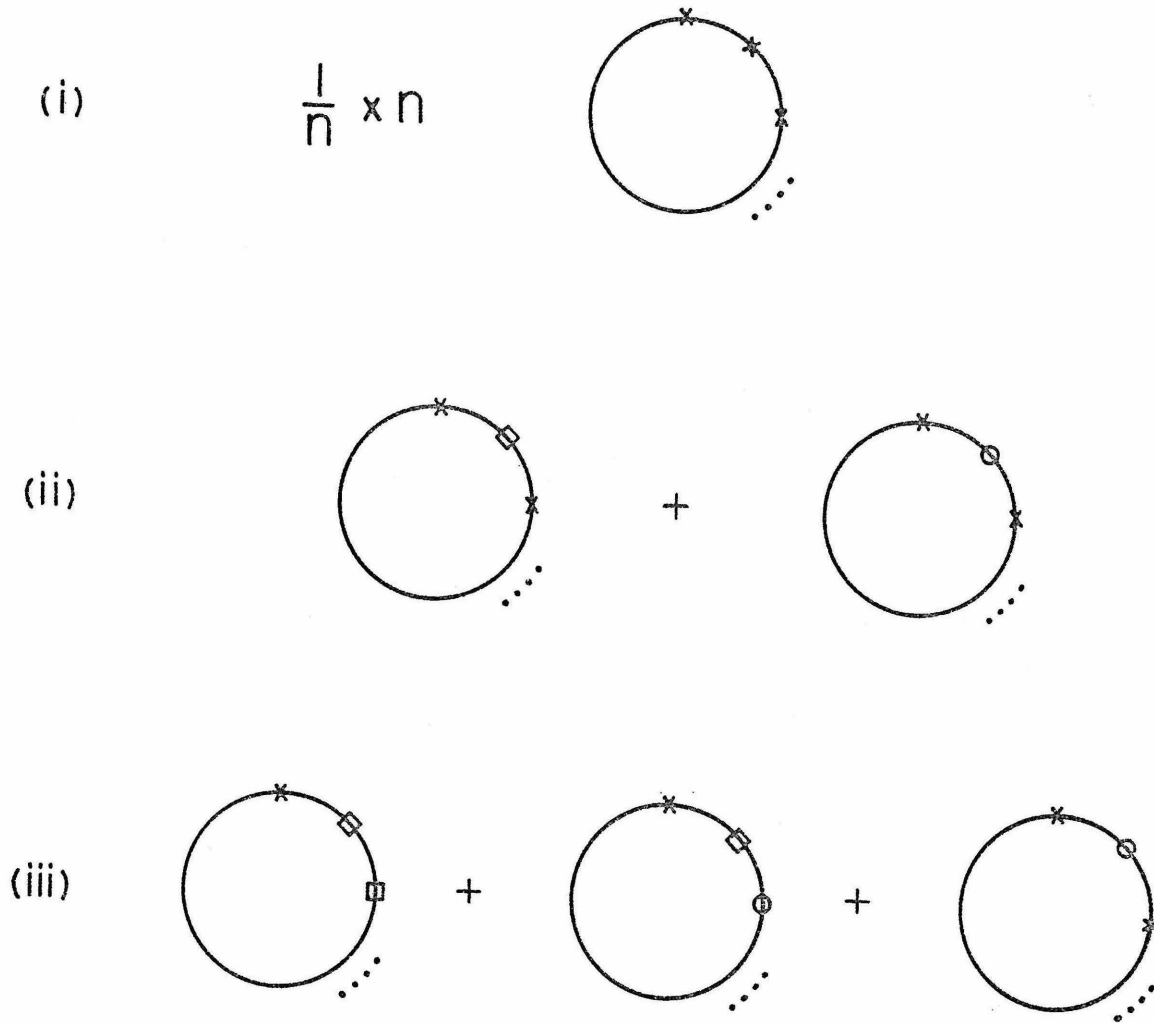


Figure 4: Illustration of the decomposition procedure (i)~(iii) of the n th term of the expansion (3.9). The solid lines denote the Green's function are particles with mass m_+ .

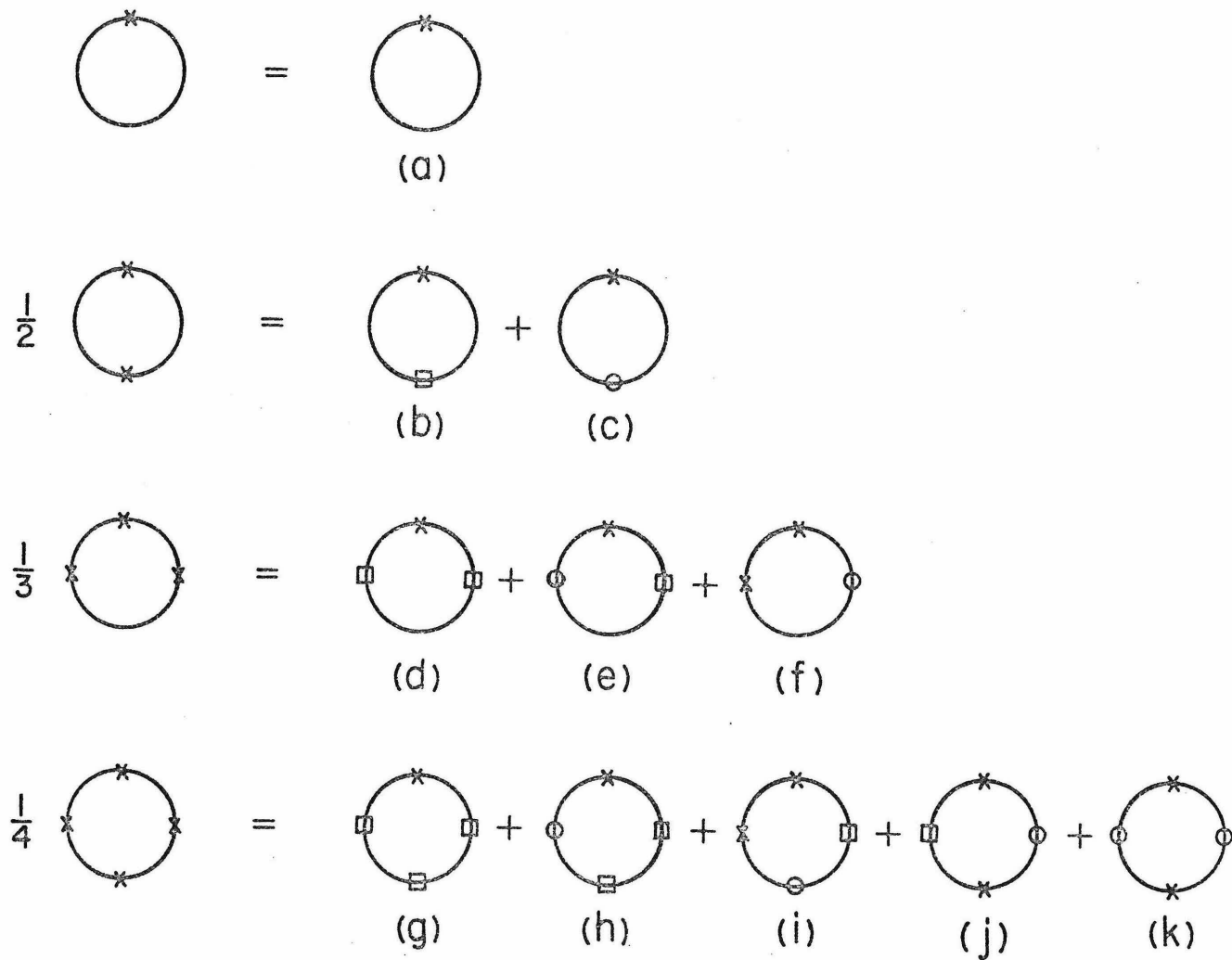


Figure 5: Decomposition of the first four terms of the expansion (3.9).

$$\sum_{l=0}^{\infty} \underbrace{\text{---} \square \text{---} \square \text{---} \dots \text{---} \square \text{---}}_l = \text{====}$$

Figure 6: The graphical representation of (3.10). The double-solid line denotes the Green's function of a particle of mass m_{-} .

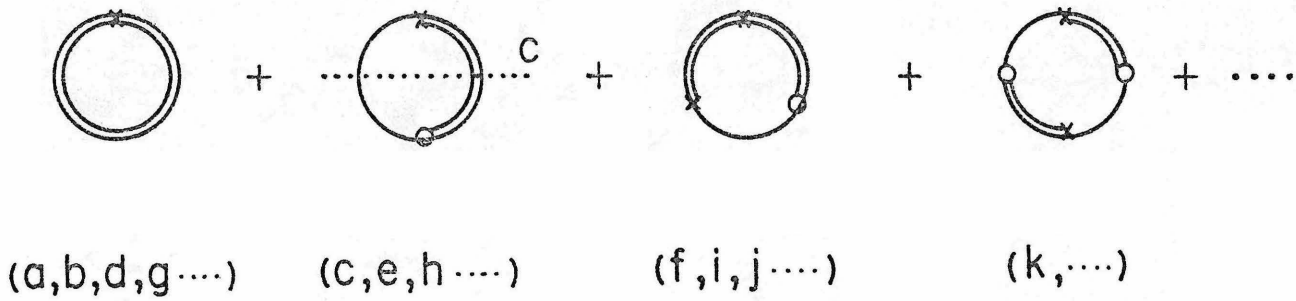


Figure 7: The rearranged series. The letters in the parentheses denote the graphs of Fig.5 which are to be included in each of the above graphs.

vertex \odot is zero where $\tilde{\varphi} = \varphi_-$. Therefore, the first graph in Fig. 7 can be understood as a quantum correction to S_{eff} due to a virtual particle exists only in the true vacuum. In the second graph, the particle goes through both the false and the true vacua. This situation is illustrated in Fig. 8 together with the interpretation of other graphs of Fig. 7.

The result of the rearrangement, Fig. 7, does not treat the two vacua equally. If we start from the perturbation expansion (3.9) with $m = m_-$, we get another set of graphs in Fig. 9. A symmetric set of graphs is obtained by averaging the graphs in Fig. 7 and Fig. 9. In any case, the lowest nontrivial graph is the second graph in Fig. 7. This graph is equivalent to the second graph in Fig. 9 and is symmetric. The cut C of this graph corresponds to a particle of mass m_+ and a particle of mass m_- . This property is desirable for dealing with the case when the bubble wall creates a pair with one particle going out and the other falling in.

The resulting effective action, in contrast to (3.10), is

$$S_{eff}[\tilde{\varphi}] = S[\tilde{\varphi}] + \left[\frac{\partial^2 V(\tilde{\varphi})}{\partial \tilde{\varphi}^2} - m_+^2 \right] K_0 \left[\frac{\partial^2 V(\tilde{\varphi})}{\partial \tilde{\varphi}^2} - m_-^2 \right], \quad (3.16)$$

where the kernel K_0 in momentum space is given by,

$$K_0(k^2) = \frac{-1}{32\pi^2} \left[\frac{1}{4\pi} \right]^\omega \Gamma(-\omega) - \frac{1}{32\pi^2} \int_0^1 dx \ln(m_+^2 x + m_-^2 (1-x) - i\varepsilon - k^2 x(1-x)).$$

The above has an imaginary part

$$\text{Im}K_0(k^2) = \frac{1}{32\pi} \mathcal{V}(k^2 - (m_+ + m_-)^2) \sqrt{1 - \frac{2(m_-^2 + m_+^2)}{k^2} - \frac{(m_+^2 - m_-^2)^2}{(k^2)^2}}.$$

The equation for the effective configuration $\tilde{\varphi}$ is obtained from (3.14).

$$-\partial_\mu \partial^\mu \tilde{\varphi} + \frac{\partial V(\tilde{\varphi})}{\partial \tilde{\varphi}} + \frac{\partial^3 V(\tilde{\varphi})}{\partial \tilde{\varphi}^3} 2K_0 \left[\frac{\partial^2 V(\tilde{\varphi})}{\partial \tilde{\varphi}^2} - \frac{m_-^2 + m_+^2}{2} \right] = 0. \quad (3.17)$$

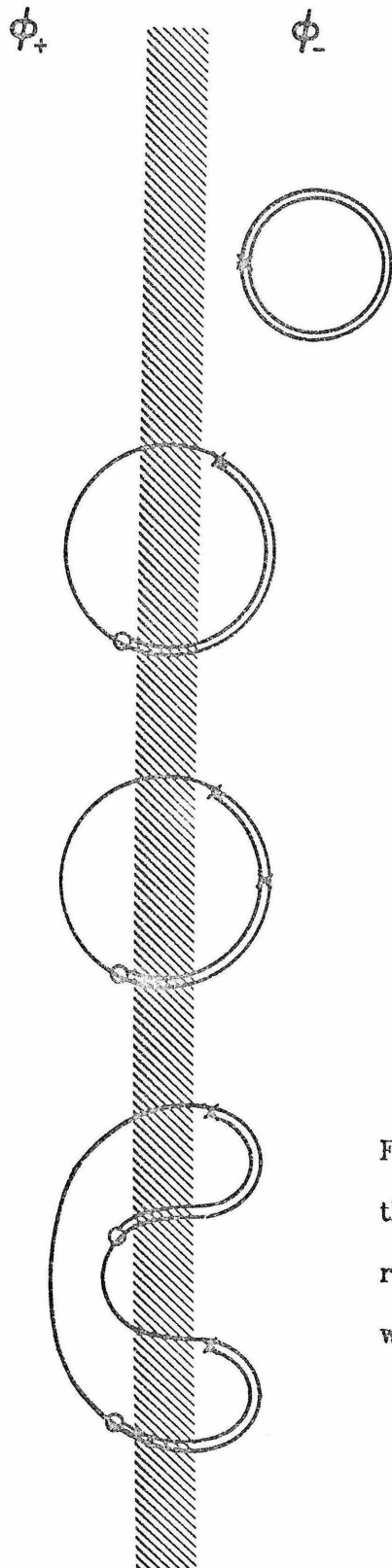


Figure 8: Space-time interpretation of the graphs in the Fig.7. The shaded region shows the transition region, the wall, between ϕ_+ and ϕ_- .

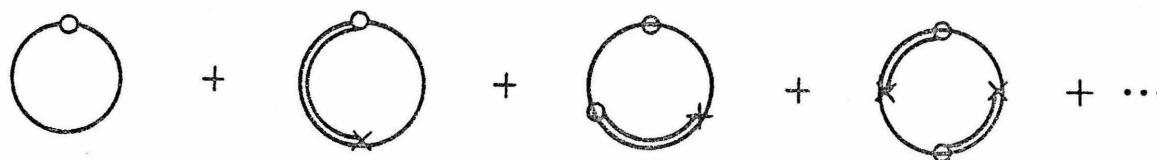


Figure 9: An another rearranged series.

The real configuration φ^r satisfies a similar equation obtained by replacing $i\varepsilon$ in K_0 by $i\varepsilon k_0$ as was done in (3.14).

In summary, the equations for each of the following three cases have been obtained; (i) both particles of a created pair going outside of the bubble, (ii) both going inside and (iii) one going outside and the other inside. All equations seem to require numerical calculations. The consistency of the behavior assumed for pair creation has to be checked. It is also possible that the physical situation is a superposition of the three states. For example, half of the pair can go inside, while the other half split. If that is the case, the equation for φ^r has to be improved further.

For the purpose of examining the features of pair production, a semi-classical method has been applied to this model by the author. In the next section, we describe the method and some of the results obtained.

4. A Semi-classical Analysis

The effective action method gives physical quantities such as the pair production probability as functionals of the effective configuration $\tilde{\varphi}$ (Section 3 of Chapter II) or the real configuration φ^r ((II.4.10) \sim (II.4.13)). The quantum correction part S^f of the effective action is a functional of $\tilde{\varphi}$. By extremizing $S + S^f$, we obtained equations for $\tilde{\varphi}$, (3.13) and (3.16). These equations, and equations for φ^r , are, in general, nonlinear integro-differential equations and therefore seem hard to treat analytically. However, if we parametrize $\tilde{\varphi}$ and φ^r and thereby reduce their degrees of freedom, then the field equations reduce to equations on the parameters, which are easier to be examined. At the classical level, the parametrization is done by using $R(t)$, the radius of the bubble at time t [5]. The behavior of the solution of the field equation φ_1 of (2.6) has been successfully reproduced by the solution (2.4) of the energy conservation law,

$$0 = E^b(T) = \frac{4\pi S_1 R^2}{\sqrt{1-R^2}} - \frac{4\pi\epsilon}{3} R^3. \quad (4.1)$$

Quantum corrections modify the energy conservation law. If pairs of particles are created, a portion of the energy released from the false vacuum is carried away by the pairs. Thus, the acceleration rate of the wall is expected to be smaller than the classical rate. As a result, the bubble expands at a slower rate than the classical rate. If we assume that with pair creation, the solution, φ^r , can still be parametrized by $R(t)$, then the energy, $E^{pair}(T)$, consumed to create pairs by time t is a functional of $R(t)$. The total energy conservation law

$$0 = E^b(T) + E^{pair}(T) \quad (4.2)$$

should yield a solution $R(t)$ that describes a slower expanding bubble.

In order to estimate $E^{pair}(T)$ in terms of $R(t)$, we have to express $\varphi^r(t, \mathbf{x})$ in terms of $R(t)$. Since the classical solution φ_1 has to be reproduced to some

accuracy in the limit $\hbar \rightarrow 0$, we first examine the properties of φ_1 and an appropriate parametrization in terms of $R(t)$. For the renormalizability of the action (2.1), $V(\varphi)$ is a fourth order polynomial in φ . Of the five possible coefficients in the polynomial, only three are physical: Since we neglect the effect of gravity, the value of V itself is unphysical, and the value φ itself is unphysical. These two redundant degrees of freedom correspond to the vertical and horizontal parallel transport of the curve $V(\varphi)$ in the V - φ plane (Fig. 1). A traditionally used set of three constants is $\{\mu, \lambda, \varepsilon_0\}$ and gives the following $V(\varphi)$ of (2.2) [16, 5, 6],

$$V(\varphi) = \frac{\lambda}{8}(\varphi^2 - a^2)^2 + \frac{\varepsilon_0}{2a}(\varphi - a), \quad (4.3)$$

with

$$a = \sqrt{\frac{\mu^2}{\lambda}}. \quad (4.4)$$

All constants are positive. For small ε_0 , the values of the φ -field in the true and false vacua are given by

$$\varphi_{\pm} = \pm a - \frac{\varepsilon_0}{2\lambda a^3} + O(\varepsilon_0^2). \quad (4.5)$$

For later convenience, we give the values of several parameters in the false and true vacua.

$$V(\varphi_+) = -\frac{\varepsilon_0^2}{8\lambda a^4} + O(\varepsilon_0^3), \quad (4.6)$$

$$V(\varphi_-) = -\varepsilon_0 - \frac{\varepsilon_0^2}{8\lambda a^4} + O(\varepsilon_0^3), \quad (4.7)$$

$$\frac{\partial^2 V}{\partial \varphi^2} = \frac{\lambda}{2}(3\varphi^2 - a^2), \quad (4.8)$$

$$m_{\pm}^2 = \left. \frac{\partial^2 V}{\partial \varphi^2} \right|_{\varphi = \varphi_{\pm}} = \lambda a^2 \mp \frac{3\varepsilon_0}{2a^2} + O(\varepsilon_0^2) = \mu^2 \mp \frac{3\varepsilon_0}{2a^2} + O(\varepsilon_0^2). \quad (4.9)$$

The difference ε of the energy densities of the false and true vacua is equal to ε_0 at the lowest order of the ε_0 -expansion.

$$\varepsilon \equiv V(\varphi_+) - V(\varphi_-) = \varepsilon_0 + O(\varepsilon_0^3). \quad (4.10)$$

Therefore, the bubble has a thin wall when ε_0 is small. Because of the mathematical simplicity, we will concern ourselves with this thin wall case.

The classical field equation (3.1) for the present V is;

$$\partial_\mu \partial^\mu \varphi_1 + \frac{\lambda}{2} \varphi_1 (\varphi_1^2 - a^2) + \frac{\varepsilon_0}{2a} = 0. \quad (4.11)$$

And for a spherically symmetric φ_1 , (4.11) reduces to

$$\left[\frac{\partial^2}{\partial t^2} - \frac{\partial^2}{\partial r^2} - \frac{2}{r} \frac{\partial}{\partial r} \right] \varphi_1 + \frac{\lambda}{2} \varphi_1 (\varphi_1^2 - a^2) + \frac{\varepsilon}{2a} = 0. \quad (4.12)$$

Consider the solution at $t = 0$, when the bubble has the minimum radius R_0 . The derivative terms of φ_1 are nonzero only near the wall. Since the bubble is expected to expand in the time scale of $\sim R_0$ according to (2.4), we have,

$$\frac{\partial^2}{\partial t^2} \varphi_1 \sim O\left(\frac{a}{R_0^2}\right).$$

By writing the width of the wall as w , we have

$$\frac{\partial^2}{\partial r^2} \varphi_1 \sim O\left(\frac{a}{w^2}\right), \quad \frac{1}{r} \frac{\partial}{\partial r} \varphi_1 \sim O\left(\frac{a}{R_0 w}\right).$$

Since we have

$$R_0 \gg w, \quad (4.13)$$

only the $\frac{\partial^2}{\partial r^2} \varphi_1$ term is dominant among the derivative terms of (4.12). Therefore, near the wall, the field equation (4.12) reduces to the following,

$$-\frac{\partial^2}{\partial r^2} \varphi_1 + \frac{\lambda}{2} \varphi_1 (\varphi_1^2 - a^2) + \frac{\varepsilon}{2a} = 0. \quad (4.14)$$

In the perturbation expansion of φ_1 in ε , the first term is known to be the following [6];

$$\varphi_1 = a \tanh \frac{\mu(r-R_0)}{2} + \varepsilon_0 f(r) + O(\varepsilon_0^2), \quad (4.15)$$

where the function $f(r)$ satisfies the following equation.

$$-\frac{\partial^2}{\partial r^2} f + \mu^2 \left[1 - \frac{3}{2} \operatorname{sech}^2 \frac{\mu(r-R_0)}{2} \right] f + \frac{1}{2a} = 0.$$

For $|\mu(r-R_0)| \gg 1$, the above equation has the solution

$$f = -\frac{1}{2a\mu^2} = -\frac{1}{2\lambda a^3}.$$

Therefore, property (2.6) can be satisfied. For $r \sim R_0$, f would have a peak of width $\sim \frac{1}{\mu}$. The resulting solution φ_1 is illustrated in Fig. 10. The solution (4.15) gives the surface tension S_1 of (2.3) as

$$S_1 = \frac{\mu^3}{3\lambda}.$$

Since R_0 is given by (2.5), we learn that

$$R_0 = \frac{\mu^3}{\lambda\varepsilon}. \quad (4.16)$$

The wall has a thickness $1/\mu$.

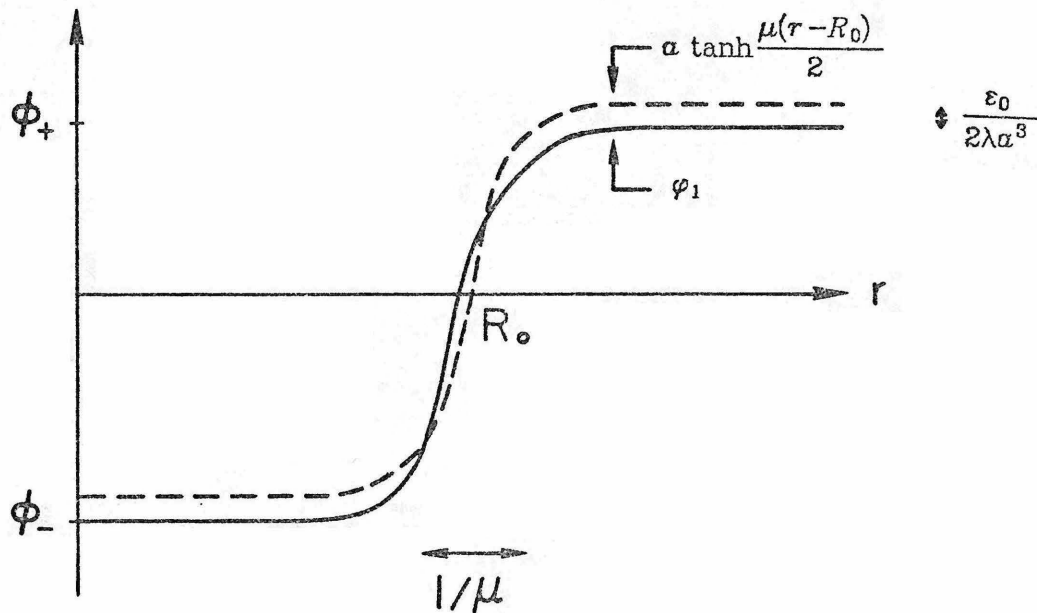


Figure 10: A possible shape of the solution (4.15) for φ_1 . The broken line gives the $O(1)$ -term of φ_1 , while the solid line includes the $O(\epsilon)$ -contribution.

Therefore, the condition for the thin wall approximation (4.13) becomes,

$$R_0 \gg \frac{1}{\mu} , \quad (4.17a)$$

or

$$R_0 \mu = \frac{\mu^4}{\lambda \varepsilon} \gg 1. \quad (4.17b)$$

As was explained in the previous section, the solution for $t \neq 0$ is obtained by substituting r by $\sqrt{r^2 - t^2}$ in φ_1 ,

$$\varphi_1 = a \tanh \frac{\mu(\sqrt{r^2 - t^2} - R_0)}{2} + \varepsilon_0 f(\sqrt{r^2 - t^2}) + O(\varepsilon_0^2), \quad (4.18)$$

which is appropriate outside the light cone ($r > |t|$). Inside the light cone, $\varphi_1 \sim \varphi_-$. It is also shown that φ_1 behaves regularly near the light cone, $r = |t|$ [22]. The resulting φ in the whole space-time is quite "clean" except for the region occupied by the wall as is shown in Fig. 2. The thickness of the wall changes with time. In fact, if we define $R(t)$ as the radius of the zero point of φ_1 , at the classical level, we have

$$\sqrt{R^{cl}(t)^2 - t^2} - R_0 = 0$$

where we neglected the $O(\varepsilon)$ term. Thus,

$$R^{cl}(t) = \sqrt{t^2 + R_0^2} .$$

Near the wall, the argument of tanh in (4.18) is approximated by the following Taylor expansion,

$$\mu(\sqrt{r^2 - t^2} - R_0) \sim \frac{\mu\sqrt{t^2 + R_0^2}}{R_0} (r - R^{cl}(t)) + O((r - R(t))^2)$$

$$\equiv \mu_t (r - R^{cl}(t)) + O((r - R(t))^2). \quad (4.19)$$

Thus, the thickness $\frac{1}{\mu_t}$ of the wall decreases with time for $t > 0$. This is understood as a result of Lorentz contraction. In fact, at any time t ,

$$\frac{1}{\mu_t} = \frac{1}{\mu} \sqrt{1 - \dot{R}^2(t)} \quad (4.20)$$

is satisfied by $R = R^{cl}$.

We assume a similar behavior for the real configuration φ^r at the quantum level,

$$\varphi^r = a \tanh \frac{\mu_t (r - R(t))}{2} + \varepsilon_0 f \left[\frac{\mu_t}{\mu} (r - R(t)) \right] + O(\varepsilon_0^2), \quad (4.21a)$$

where μ_t is given by (4.20). Since the bubble is to be created at $t \sim 0$, (4.21a) should apply for $t \gtrsim 0$. For $t \lesssim 0$,

$$\varphi^r = \varphi_+. \quad (4.21b)$$

The assumption (4.21a, b) reduces the problem of finding $\varphi^r(r, t)$ to the problem of finding $R(t)$, thus simplifying the problem. The region $t \sim 0$ needs a careful consideration. If the bubble is created spontaneously, i.e., via a quantum tunneling, just after its birth, space has to be clean; there should be no particles. Therefore, the end point $t \sim 0$ of the bubble world sheet should not create any pairs. The right prescription for treating this region $t \sim 0$ is not known. Our aim here in this section is to obtain results that are insensitive to the region $t \sim 0$.

Because of (II.4.b a), the physical observables that are related to pair creation, but not to pair annihilation, can be directly calculated in terms of φ^r .

Examples are given in (II.4.12) and (II.4.13). For the purpose of obtaining $E^{pair}(T)$, the energy carried away by the created pairs, in terms of $R(t)$, we first consider the creation probability $P(k)$ of a pair of the total four momentum k ,

$$P(k) = R(k^2)e^{-R},$$

with

$$R(k^2) = \left[\frac{\partial^2 V(\varphi^r)}{\partial \varphi^{r^2}} - m^2 \right] 2 \operatorname{Im} K_0(k^2) \left[\frac{\partial^2 V(\varphi^r)}{\partial \varphi^{r^2}} - m^2 \right], \quad (4.22)$$

and

$$R = \int d^4k R(k^2). \quad (4.23)$$

In the above, as was explained in the previous section, m takes the value of either m_+ or m_- depending on different physical situations. Summing over the incoherent production probabilities, we learn that the pair energy $E^{pair}(\infty)$ is given by the following,

$$\begin{aligned} E^{pair}(\infty) &= \int d^4k |k^0| R(k^2) e^{-R} + \dots + \frac{1}{n!} \int \prod_{i=1}^n d^4k_i R(k_i^2) \left[\sum_{l=1}^n |k_l^0| \right] e^{-nR} + \dots \\ &= \int d^4k |k^0| R(k^2), \end{aligned} \quad (4.24)$$

where we have used (4.23).

At the lowest order of ε_0 , the vertex in (4.22) is given as follows,

$$\begin{aligned} \frac{\partial^2 V(\varphi^r)}{\partial \varphi^{r^2}} - m^2 &= \frac{3\lambda}{2} (\varphi^{r^2} - a^2) + O(\varepsilon_0) \\ &= -\frac{3\mu^2}{2} \vartheta(t) \operatorname{sech}^2 \frac{\mu_t(r - R(t))}{2} + O(\varepsilon). \end{aligned} \quad (4.25)$$

At this order, there is no actual distinction between three cases; (i) both particles of a pair go outside the bubble, (ii) both particles of a pair go inside the bubble, (iii) one outside and the other inside. This is because for $\varepsilon_0 = 0$, the potential (4.3) is symmetric, $m_+ = m_-$, and therefore particles do not distinguish true vacuum from false vacuum. The energy-density difference ε_0 appears only in the expression of the bubble energy (4.1).

The pair energy $E^{pair}(\infty)$ is now explicitly given as follows,

$$E^{pair}(\infty) = \int d^4x \int d^4x' \int \frac{d^4k}{(2\pi)^4} |k^0| 2\text{Im}K_0(k^2) e^{ik(x-y)} V(x,t) V(x',t') + O(\varepsilon_0) \quad (4.26)$$

where,

$$V(x,t) \equiv -\frac{3\mu^2}{2} \vartheta(t) \text{sech}^2 \frac{\mu_i(r-R(t))}{2}. \quad (4.27)$$

Since $\text{Im}K_0(k^2)$ is not polynomial in k^2 as is seen in (3.12), its Fourier transform is nonlocal, in contrast to the model discussed in the previous chapter (see (III.2.7) and (III.2.9)). This causes difficulty in finding the $E^{pair}(t)$ for finite t : If $E^{pair}(\infty)$ is expressed by a one-fold integration over a time coordinate t , $E^{pair}(T)$ is given by the finite integration of the same integrand with upper limit T . This prescription is not applicable to our case. In order to define $E^{pair}(T)$ for a finite T , we introduce a cutoff function

$$e^{-\frac{t}{T}} \quad (4.28)$$

for each of the vertices in (4.26). Since this cutoff function gradually turns off the vertices after $t \sim T$, the resulting integration seems appropriate for the definition of $E^{pair}(T)$, the energy carried away by the created pairs by time T .

Another reason for choosing (4.28) is that the integral in (4.26) is actually divergent because of the upper limit $t \sim t' \sim \infty$. Consider a case when $E^{pair}(T)$ is a single-fold integration over t and is divergent, for example,

$$E^{pair}(\infty) = A \int_0^\infty dt t^n \quad (n > 0).$$

In this case, exact E^{pair} for a finite T is given by

$$E^{pair}(T) = A \int_0^T dt t^n = \frac{AT^{n+1}}{n+1}.$$

The cutoff function (4.28) gives the following approximation for the above $E^{pair}(T)$,

$$E^{pair}(T) \cong A \int_0^\infty dt t^n e^{-\frac{t}{T}} = A n! T^{n+1}.$$

Therefore, the asymptotic behavior of $E^{pair}(T)$ is correctly reproduced. However, the example also shows that the numerical factor in the result obtained under our assumption should not be rigorously believed in.

We limit ourselves with the asymptotic behavior of E for the following reasons: (i) We do not know how to treat the region $t \sim 0$, where quantum tunneling is essential. Thus, we need a result that is insensitive to that region. (ii) When $T \sim 0$, our cutoff (4.26) is not smooth and thus inappropriate. This limit is nevertheless interesting because the asymptotic behavior of the bubble expansion is important for cosmological problems.

The integral over x and x' in (4.26) is straightforward.

$$\begin{aligned} \check{V}_T(k, k_0) &\equiv \int d^4x e^{ikx} V(x, t) \\ &= -24\pi^2 \mu^2 \int_0^\infty dt e^{-\frac{t}{T} + ik_0 t} \frac{R_t}{\mu_t^2} \sin k_r R_t \operatorname{cosech} \frac{\pi k_r}{\mu_t} + \dots \end{aligned} \quad (4.29)$$

with $R_t \equiv R(t)$ and $k_r \equiv |k|$, and we kept only the leading term in the thin wall approximation. The following formula has been used to derive (4.29) [23],

$$\int_{-\infty}^{\infty} dr \cos k_r r \left[\operatorname{sech} \frac{\mu_t r}{2} \right]^{2n} = \frac{4^n \pi k_r}{(2n-1)! \mu_t^{2n}} \operatorname{cosech} \frac{\pi k_r}{\mu_t} \prod_{l=1}^{n-1} \left[\frac{k_r^2}{\mu_t^2} + l^2 \right]. \quad (4.30)$$

In order to evaluate (4.29), we assume that the asymptotic speed β of the bubble expansion is less than 1, the speed of light,

$$R(t) \rightarrow \beta t + \dots \quad \text{as } t \rightarrow \infty. \quad (4.31)$$

In this case, (4.29) is approximated as follows,

$$\begin{aligned} \tilde{V}_T(k_r, k_0) &\cong - \frac{24\pi^2 \mu^2 \beta}{\mu_\infty^2} \operatorname{cosech} \frac{\pi k_r}{\mu_\infty} \int_0^\infty dt e^{-\frac{t}{T} + ik_0 t} t \sin k_r \beta t \\ &= -24\pi^2 (1-\beta^2) \beta \operatorname{cosech} \frac{\pi k_r}{\mu_\infty} \left[\frac{-2ik_0 k_r \beta}{(k_0^2 - k_r^2 \beta^2)^2} + O\left(\frac{1}{T}\right) \right]. \end{aligned} \quad (4.32)$$

The pair energy E^{pair} is calculated from the following formula,

$$E^{pair}(T) = \frac{1}{32\pi^4} \int_{2\mu}^\infty k_0 dk_0 \int_0^{\sqrt{k_0^2 - 4\mu^2}} k_r^2 dk_r \sqrt{1 - \frac{k^2}{4\mu^2}} |\tilde{V}_T(k_r, k_0)|^2, \quad (4.33)$$

where we have used (3.12) and (4.26). The vertex (4.32) leads to the following,

$$\begin{aligned} E^{pair}(T) &= 288\pi^4 (1-\beta^2)^2 \beta^4 \int_{2\mu}^\infty k_0 dk_0 \int_0^{\sqrt{k_0^2 - 4\mu^2}} k_r^2 dk_r \sqrt{1 - \frac{k^2}{4\mu^2}} \\ &\quad \times \left[\operatorname{cosech} \frac{\pi k_r}{\mu_\infty} \right]^2 \frac{k_0^2 k_r^2}{(k_0^2 - k_r^2 \beta^2)^4} + O\left(\frac{1}{T}\right). \end{aligned} \quad (4.34)$$

This yields a finite result. The integrand in (4.34) has no singularity in the integration region because the denominator, $k_0^2 - k_r^2 \beta^2$, is always greater than $4\mu^2$. For $k_0 \rightarrow \infty$, the k_r -integration is finite because of the $(\operatorname{cosech})^2$. Thus, the k_0 -integration

k_0 -integration becomes

$$\sim \int^{\infty} k_0 dk_0 \frac{k_0^2}{k_0^3} (\mu_{\infty})^5, \quad (4.35)$$

which is finite for $\beta < 1$. The pair energy $E^{pair}(\infty)$ is approximately

$$E^{pair}(\infty) \sim \frac{9}{64} \frac{\beta^4}{\sqrt{1-\beta^2}} \mu. \quad (4.36)$$

Since $E^{pair}(T)$ is finite for $T \rightarrow \infty$, we conclude that the asymptotic speed of the bubble expansion cannot be less than 1. Consider r.h.s. of the equation (4.2),

$$\frac{4\pi S_1 R_T^2}{\sqrt{1-R_T^2}} - \frac{4\pi\epsilon}{3} R_T^3 + E^{pair}(T). \quad (4.37)$$

Using the asymptotic form (4.31) for R_T , we learn that as $T \rightarrow \infty$, the leading orders of the first and second terms are of $O(T^2)$ and $O(T^3)$, respectively. Since we have found that $E^{pair}(T)$ is of $O(1)$ in this case, it is impossible to balance the released energy (the second term) with the pair energy, i.e., we cannot have zero coefficient for the leading $O(T^3)$ term in (4.37). Therefore, the asymptotic behavior (4.31) cannot be a self-consistent asymptotic solution of (4.2).

Next, we consider the case when the asymptotic expansion speed is 1. Naively, (4.36) gives a divergent expression and therefore suggests that pair creation may affect the expansion rate significantly. The classical solution $R^{cl}(t)$ has the following asymptotic behavior,

$$R^{cl}(t) = \sqrt{t^2 + R_0^2} \rightarrow t + \frac{R_0^2}{2t} + \dots \quad (4.38)$$

We assume a similar asymptotic behavior for $R(t)$,

$$R(t) \rightarrow t + a + \frac{b^2}{2t} + \dots \quad (4.39)$$

Since, in this case,

$$\dot{R}(t) \rightarrow 1 - \frac{b^2}{2t^2}, \quad (4.40)$$

we expect that $b > R_0$, so that the expansion is slowed down by pair creation.

The vertex \tilde{V} of (4.29) is now,

$$\tilde{V}_T(k_r, k_0) \cong -24\pi^2 b^2 \int_0^\infty dt e^{-\frac{t}{T} + ik_0 t} \frac{\sin k_r t}{t} \operatorname{cosech} \frac{\pi b k_r}{\mu t}, \quad (4.41)$$

where we have used

$$\mu_t \rightarrow \mu \frac{t}{b}. \quad (4.42)$$

In order to estimate (4.40) and $E^{\text{pair}}(T)$ of (4.33), we divide the momentum space integral in (4.33) into two parts.

$$(1) T \gtrsim \frac{\pi b k_r}{\mu}.$$

The integration is dominated by the region where the argument of cosech is small. Thus, by approximating $\operatorname{cosech} x \sim 1/x$, we get

$$\tilde{V}_T(k_r, k_0) \cong -24\pi b\mu \frac{1}{\left(\frac{1}{T} - ik_0\right)^2 + k_r^2}.$$

Therefore, the total energy $E^{\text{pair},1}(T)$ of the pairs created in this region, i.e.,

$|\text{total three-momentum}| \lesssim \frac{\mu T}{\pi b}$, is given as follows,

$$E^{\text{pair},1}(T) \cong \frac{18}{\pi^2} \mu^2 b^2 \int_0^{\frac{\mu T}{\pi b}} k_r^2 dk_r \int_{\sqrt{k_r^2 + 4\mu^2}}^\infty k_0 dk_0 \sqrt{1 - \frac{4\mu^2}{k^2}} \left| \frac{1}{\left(\frac{1}{T} - ik_0\right)^2 + k_r^2} \right|^2. \quad (4.43)$$

The k_0 -integration is finite for $T \rightarrow \infty$. An approximate value $1/8\mu^2$ is obtained if we neglect the $\sqrt{\cdot}$ -function that is $\cong 1$ except near the boundary, $k^2 = 4\mu^2$. Note that the main contribution comes from the peak of the integrand at $k^2 = 5\mu^2$, and the integrand k_r^2 in the k_r -integration gives the largest contribution at the upper limit $k_r \sim \frac{\mu T}{\pi b}$. The approximate value of the leading order term of (4.43) is,

$$E^{pair,1}(T) \cong \frac{3}{4\pi^5} \frac{\mu^3}{b} T^3. \quad (4.44)$$

$$(2) \quad T \lesssim \frac{\pi b k_r}{\mu}.$$

Using $\text{cosech } x \sim 2e^{-x}$ for $x \gg 1$, we approximate (4.41) as follows,

$$\tilde{V}_T(k_r, k_0) \cong -48\pi^2 b^2 \int_0^\infty dt e^{-\frac{t}{T} + ik_0 t} \frac{1}{t} \sin k_r t e^{-\frac{\pi b k_r}{\mu t}}.$$

This integration is given in terms of a modified Bessel function of the third kind, $K_0(z)$. The argument z satisfies the following,

$$|z| > 2\sqrt{2\pi\mu b} > 2\sqrt{2\pi\mu R_0} \gg 1 \quad .$$

where we used (4.17a). By using the asymptotic expansion of

$K_0(z) \sim \sqrt{\frac{\pi}{2z}} e^{-z}$, we obtain the following $E^{pair,2}(T)$,

$$E^{pair,2}(T) \cong 72\pi b^4 \int_{\frac{\mu T}{\pi b}}^\infty k_r^2 dk_r \int_{\sqrt{k_r^2 + 4\mu^2}}^\infty k_0 dk_0 \sqrt{1 - \frac{4\mu^2}{k^2}} \frac{e^{-y}}{\sqrt{2}y} e^{-\frac{8\pi^2 b^2 k_r^2}{\mu^2 T^2 y^3}},$$

where $y \equiv 2\sqrt{k_r(k_0 - k_r)} \frac{2\pi b}{\mu}$. By changing the integration variable k_0 to y , we obtain the leading order term,

$$(4.45)$$

$$E^{pair,2}(T) \approx \frac{9}{4\pi^{3/2}} (\mu b)^{7/2} e^{-2\sqrt{\pi\mu b}} \mu^4 T^3 \quad . \quad (4.45)$$

We can now discuss the consequences of the energy conservation. The asymptotic behavior (4.39) leads to the following leading terms for each piece of (4.37),

$$\text{the surface energy : } \frac{4\pi S_1 R_T^2}{\sqrt{1-R_T^2}} \rightarrow \frac{4\pi S_1}{b} T^3,$$

$$\text{the volume energy : } -\frac{4\pi\varepsilon}{3} R_T^3 \rightarrow -\frac{4\pi\varepsilon}{3} T^3.$$

The pair energy $E^{pair,2}(T)$ is considerably smaller than $E^{pair,1}(T)$ because of the factor $e^{-2\sqrt{\pi\mu b}}$, therefore we neglect $E^{pair,2}(T)$ and write

$$E^{pair}(T) \rightarrow \frac{3}{4\pi^5} \frac{\mu^3}{b} T^3.$$

The total energy conservation law (4.2) implies the following equation for b ,

$$\frac{4\pi S_1}{b} - \frac{4\pi\varepsilon}{3} + \frac{3}{4\pi^5} \frac{\mu^3}{b} = 0. \quad (4.46)$$

Thus, we obtain

$$b = R_0 \left[1 + \frac{9\lambda}{16\pi^6} \right] \quad , \quad (4.47)$$

in agreement with the naive expectation $b > R_0$. From (4.47), we also learn that the ratio of the energy used to create pairs and the released energy is given by the following.

$$\frac{\frac{9\lambda}{16\pi^6}}{1 + \frac{9\lambda}{16\pi^6}} \quad . \quad (4.48)$$

The spectrum of the created particles can be obtained from the following argument: In deriving $E^{pair,1}(T)$ of (4.44), we first learned that the integration in (4.43) is dominated by the peak, $k^2 = 5\mu^2$, of the integrand. This is mainly because of the fractional function in the integrand, which is for $T \rightarrow \infty$, $1/(k_0^2 - k_r^2)^2$. If we leave an angle ϑ between x and k unintegrated, (4.29) leads to

$$\tilde{V}_T \propto \int d(\cos\vartheta) \frac{1}{(k_0 - k_r \cos\vartheta)^2}.$$

Therefore, the integrand of (4.43) is proportional to the following,

$$\int d(\cos\vartheta) \int d(\cos\vartheta') \frac{1}{(k_0 - k_r \cos\vartheta)^2 (k_0 - k_r \cos\vartheta')^2}.$$

Thus, the peak of the integrand in (4.45) comes from the region where $\vartheta \sim \vartheta' \sim 0$. Therefore, we conclude that pair creation is a local phenomenon and that the direction of the total three-momentum of a pair is along the radius vector of the place where the pair is created, and outward. The momentum of the individual pair is obtained by noting that pair creation occurs isotopically in the rest frame of the center of mass system of the pairs. Note that it is not the rest frame of the portion of the bubble wall where a pair is created. Since $k^2 \sim 5\mu^2$ and $k_r \sim \frac{\mu T}{\pi b}$, where b is given by (4.47), the speed v of the rest frame of the center of mass system of the pairs at time T is given as follows,

$$v = \frac{k_r}{k_0} \sim 1 - \frac{5\pi^2 b^2}{2T^2}. \quad (4.49)$$

Comparing this with (4.40), we learn that v is smaller than \dot{R} . In this rest frame, the particle has an energy of $\frac{\sqrt{5}}{2}\mu$, and the velocity is $\frac{1}{\sqrt{5}}$. Therefore, the highest velocity of a particle going outward is given by

$$1 - \frac{1 - \frac{1}{\sqrt{5}}}{1 + \frac{1}{\sqrt{5}}} \frac{5\pi^2 b^2}{2T^2} \sim 1 - 9.4 \frac{b^2}{T^2}, \quad (4.50)$$

which is still smaller than \dot{R} . From this, we conclude that the created pairs are left behind the wall, i.e., inside the bubble, even though they are going outward. They have high energies of $\sim \frac{\mu T}{\pi b}$. This is consistent with the cutoff (4.28): Since the high energy component is dominant, the short time scale is important, which is not affected by the cutoff (4.28). Also, from (4.42), we learn that $k_r \sim \frac{\mu_t}{\pi}$. This agrees with the naive expectation that the thickness of the wall at T determines the scale of the energy spectrum of created pairs at T .

Some comments follow:

(i) So far, we have neglected $O(\varepsilon)$ terms in the vertex $V(x, t)$ of (4.25). From (4.15), they are

$$3\lambda\varepsilon_0 f \tanh \frac{\mu(r-R_0)}{2} + \text{constants}. \quad (4.51)$$

Consider approximating f by 1, a constant. The Fourier transform of the above has then one less power of k than the leading term in (4.29) because \tanh is an integration of sech^2 in coordinate space. Therefore, (4.51) only contributes an $O(T^2)$ term in E^{pair} . Actually, f has a "bump" at the wall. To carry the discussion further, we need to know the high momentum behavior of the Fourier transform of f .

(ii) We have also neglected the real part of the quantum correction to S_{eff} . If the shape of the potential is significantly changed by taking it into account, then assumption (4.21a) may be inappropriate. Also in a case when we consider a one-loop effective action as a starting point, the effective potential is usually not

a polynomial in φ , and (4.21a) would not be applicable. As an example, consider a case when the vertex $V(x, t)$ behaves like $\sim \text{sech}^{2n}$ instead of $\sim \text{sech}^2$ in (4.25) and (4.27). Formula (4.30) tells us that the Fourier transform has then an extra factor $k^{2(n-1)}$. In this case, the assumption on the asymptotic behavior (4.39) leads to

$$E^{pair} \propto T^{1+2n}. \quad (4.52)$$

For $n > 1$, too much energy is used to create pairs and we cannot find a solution consistent with the assumption (4.39). This kind of wall cannot attain a terminal speed smaller than 1 either, because under (4.31), k_τ -integration is finite regardless of the power of k_τ and thus E^{pair} is always finite. An alternative is to assume that

$$R(t) \rightarrow t - \eta T^\xi$$

hoping to find self-consistent values of parameters η and ξ that should satisfy $\eta\xi > 0$ and $1 > \xi > -1$. However, this assumption only changes the power of $k_0 - k_\tau$ and thus does not change the behavior indicated in (4.52). Therefore, it becomes necessary to take into account the change of the shape of the wall (sech^{2n}) itself. A possibility is that the shape, sech^{2n} , is broadened by pair creation such that $n \rightarrow 1$ when we have a self-consistent solution.

5. Discussion

The semi-classical analysis given in Section 4 showed that the Higgs particles, the excitations of the φ -field, are actually created, and as a result, the bubble expansion velocity approaches to the velocity of light slower than the classical velocity. The ratio of the energy carried by created pairs and the energy released from the false vacuum is constant in time and is given in terms of a coupling constant of the model ((4.48)). We also showed that these particles remain inside the bubble. Therefore, it is plausible that equations (3.13) and (3.14) for $m = m_-$ are the most suitable ones for the physical situation. The author has inserted the assumption (4.21a) into the field equation for the real configuration obtained from (3.13) and (3.14). That, however, does not work, because φ^r is not equal to its vacuum values inside and outside the bubble due to the presence of the produced particles. Therefore, we may have to proceed to a numerical calculation.

In Chapter IV, we have treated only quantum effects due to Higgs particles. However, the effects of other particles can be treated in a similar manner. For example, if a fermion field ψ has a Yukawa-interaction $g\bar{\psi}\psi\varphi$ with the φ -field, the vertex V is linear in φ^r . Therefore, according to the semi-classical analysis given in the previous section, this vertex has a lower power of k_r , and therefore we expect that the energy consumed to create fermion pairs is of order T^1 . However, this may not be true if the fermion is massless in one of the vacua. In such a case, if we assume that both fermion and antifermion are created in the vacuum where they are massless, the appropriate imaginary part of the loop graph has $\vartheta(k^2)$ instead of $\vartheta(k^2-4m^2)$ in (3.12). Therefore, the fraction in (4.43) has a singularity at the boundary. This divergence increases the power of T in E^{pair} . Furthermore, analyses in the previous section showed that the rest frame of the pair is, in the bubble rest frame, moving outward. Therefore, if the pair is

to be massless, it is most likely that both of the particles go outside the bubble. In usual theories, the false vacuum corresponds to the symmetric phase. Thus, the particles tend to be massless in the false vacuum. Therefore, the creation of massless particles going outside the bubble may be significant during the bubble expansion. Investigation along this line is under way.

References for Chapter IV

- [1] See, for example, S. Coleman, "The Uses of Instantons," (1977 International School of Subnuclear Physics, Ettore Majorana); T. Eguchi, P. B. Gilkey and A. J. Hanson, Phys. Rep. 66 (1980) 213.
- [2] T. Inoue, Prog. Theor. Phys. 59 (1978) 986; Y. M. Cho, Phys. Lett. 81B (1979) 25.
- [3] G. t'Hooft, Nucl. Phys. B79 (1974) 276; A. M. Polyakov, Zh. Eksp. Toer. Fiz. Pis'ma Red. 20 (1974) 430 [JETP Lett. 20 (1974) 194].
- [4] J. S. Langer, Ann. of Phys. 41 (1967) 108, gives a mathematical treatment of nucleation phenomena in the statistical physics.
- [5] M. B. Volosin, I. Yu. Kobzarev and L. B. Okun, Yad. Fiz. 20 (1974) 1229 [Sov. J. Nucl. Phys. 20 (1975) 644].
- [6] S. Coleman, Phys. Rev. D15 (1977) 2929.
- [7] G. C. Callan and S. Coleman, Phys. Rev. D16 (1977) 1762.
- [8] A. D. Linde, Phys. Lett. 100B (1981) 37.
- [9] D. A. Kirzhnits and A. D. Linde, Phys. Lett. 42B (1972) 471, Ann. Phys. 101 (1976) 195; L. Dolan and R. Jackiw, Phys. Rev. D9 (1974) 3320; S. Weinberg, Phys. Rev. D9 (1974) 3357.
- [10] P. A. M. Dirac, Phys. Rev. 74 (1948) 817; G. t'Hooft, Nucl. Phys. B79 (1974) 276, B105 (1976) 538; A. M. Polyakov, Pisma Zh. Exsp. Theor. Fiz. 20 (1974) 430 [JETP Lett. 20 (1974) 194].
- [11] Ya. B. Zeldovich and M. Yu. Khlopov, Phys. Lett. 79B (1978) 239; J. P. Preskill, Phys. Rev. Lett. 43 (1979) 1365.

- [12] A. H. Guth and S. H. Tye, Phys. Rev. Lett. 44, (1980) 631, 963; A. H. Guth, Phys. Rev. D23, (1981) 347; A. H. Guth and E. J. Weinberg, Phys. Rev. D23, (1981) 876.
- [13] S. W. Hawking, I. G. Moss and J. M. Stewart, "Bubble Collisions in the Very Early Universe," Cambridge (PAMTP) preprint.
- [14] A. D. Linde, Phys. Lett. 108B, (1982) 389.
- [15] S. W. Hawking and I. G. Moss, Phys. Lett. 110B, (1982) 35.
- [16] T. D. Lee and G. C. Wick, Phys. Rev. D9, (1974) 2291.
- [17] S. Coleman, V. Glaser and A. Martin, Commun. Math. Phys. 58, (1978) 211.
- [18] A. M. Polyakov, Nucl. Phys. B120, (1977) 429.
- [19] C. De Dominicis and P. C. Martin, J. Math. Phys. 5, (1964) 14, 31; R. Jackiw, Phys. Rev. D6, (1973) 1686.
- [20] Y. Nambu, Phys. Lett. 26B, (1966) 626; L. S. Brown and D. Boulusare, Phys. Rev. 172, (1968) 1628.
- [21] H. Aoyama, unpublished.
- [22] R. F. Sawyer, UCSB preprint TH-53 (1982).
- [23] "Table of Integral Transforms" (Bateman Manuscript Project) vol.1, page 30 (McGraw-Hill,1954).